electrochemical surface science

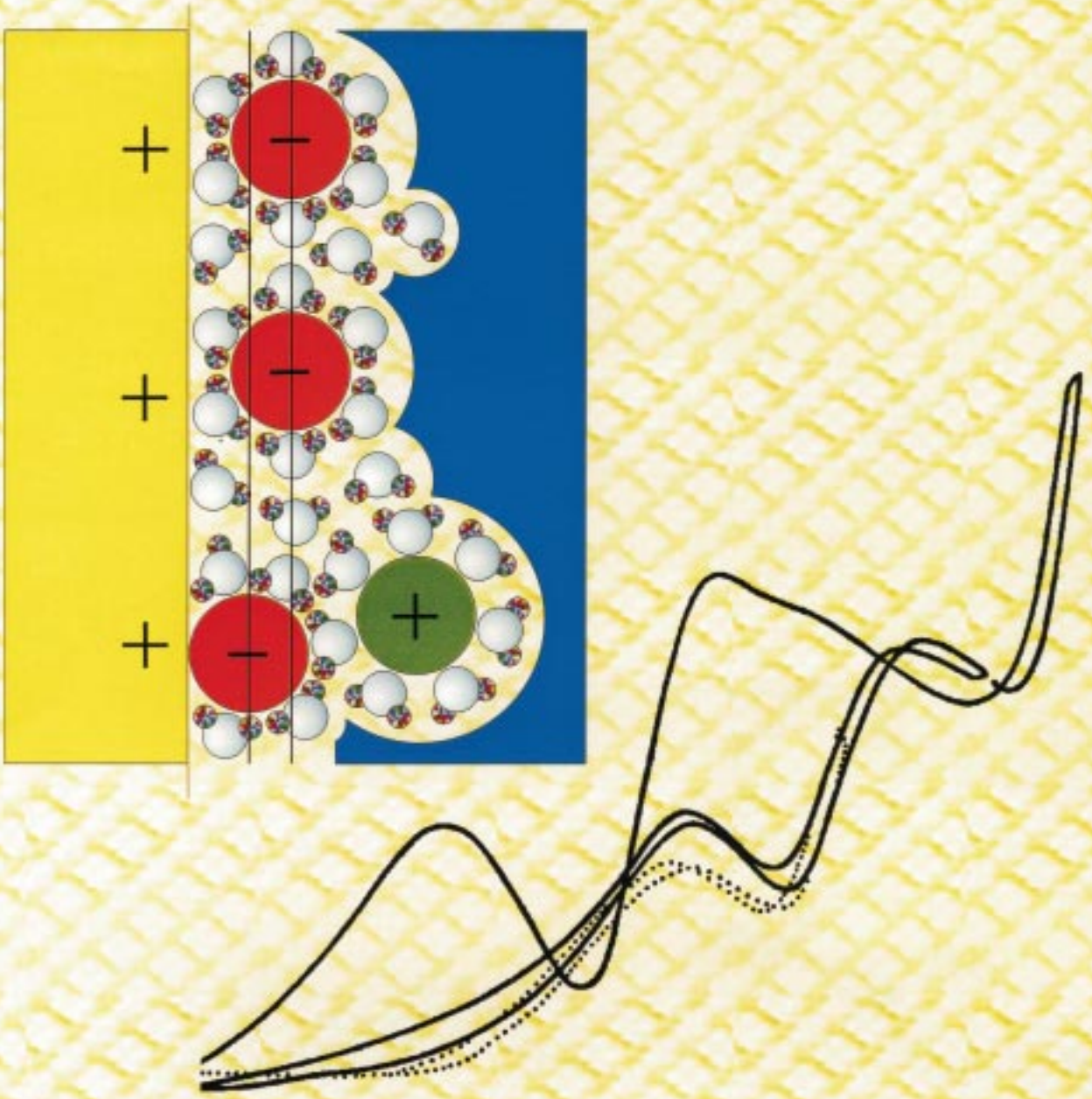

Electrochemical Surface Science**

Dieter M. Kolb*

The last 30 years have seen remarkable changes in interfacial electrochemistry, particularly in the kind of questions that were addressed in electrochemical studies. Ever since classical surface science, traditionally performed under ultrahigh vacuum conditions, has succeeded in describing surfaces and surface reactions on a molecular level, electrochemists longed for a microscopic understanding of the solid/electrolyte interface and, at the same time, searched widely for new experimental ways to reach that goal. Herein, studies are described concerning the structure and the dynamics of bare and adsorbate-covered electrode surfaces and of metal deposition as a simple, yet important, electrochemical process. In all these cases, the scanning tunneling microscope plays a pivotal role emphasizing the surface-science approach to the problems.

Keywords: electrochemistry · scanning tunneling microscopy · surface analysis · surface structure

1. Introduction

Electrochemistry deals in the widest sense with chemical reactions that are connected with the transfer of electric charge. Typical examples are the oxidation (reduction) of Fe^{2+} (Fe^{3+}) [Eq. (1)] or the oxidation or deposition of a metal from solution [Eq. (2)].

$$Fe^{2+}_{solv} \rightleftarrows Fe^{3+}_{solv} + e^{-}_{metal} \quad (1)$$

$$Cu \rightleftarrows Cu^{2+}_{solv} + 2e^{-}_{metal} \quad (2)$$

The former is an electron-transfer reaction; the latter an ion-transfer reaction. Such reactions occur normally at the interface between an electrode, which in most cases is an electronic conductor, and the electrolyte, an ionic conductor. The electrochemical reaction acts as a switch between both types of conductivity and allows an electric current to pass the interface (faradaic current). In the absence of an electrochemical reaction, the interface blocks charge transport, behaving like a capacitor that can be charged or discharged (capacitive current). Electrochemical reactions can be driven and controlled by applying a voltage between the (working) electrode and a counter electrode, or—if the reactions occur spontaneously—can provide electric current.[1–3]

The traditional way of studying electrochemical processes is to measure currents and voltages. Both quantities, which can be easily determined with high precision, are inherently suited to monitor the reaction and to almost uniquely classify the electrochemical system. With the development of a sophisticated thermodynamic treatment for the interface between a mercury electrode and an aqueous solution by D. C. Grahame,[4] bare and adsorbate-covered surfaces (of Hg) could be described precisely in terms of surface energies and surface excesses as a function of the applied potential.[5, 6] With the development of instationary current and voltage techniques, reactions could be described by formal reaction kinetics.[7, 8] The classical electrochemical methods laid the basis for a thermodynamic and formal-kinetics description of electrochemical processes and hence were—and still are—invaluable for the field. The models derived from such measurements, such as the electric double layer, however, were largely phenomenological.[9] Nevertheless, they seemed to work and thereby served the purpose.

In the mid-1960s, surface science began to demonstrate its potential for providing information about solid surfaces on an atomic or molecular level. With an ever-increasing number of structure-specific and surface-sensitive techniques, mainly based on the electron as a probe (photoelectron spectroscopy and electron diffraction), detailed insights on ordered adsorption (superlattices), adsorption sites, surface band structures, bond lengths and so forth were obtained.[10, 11] Of course, all these studies were performed under ultrahigh vacuum conditions (UHV) and hence were not directly applicable to electrochemical systems. Nevertheless, this surface science

[*] Prof. Dr. D. M. Kolb
Abteilung Elektrochemie
Universität Ulm
89069 Ulm (Germany)
Fax: (+49) 731-502-5409
E-mail: dieter.kolb@chemie.uni-ulm.de

[**] This manuscript is based on the Bonhoeffer–Eucken–Scheibe lectures of the Deutsche Bunsengesellschaft, given by the author at Erlangen, Berlin, and Leipzig in 1999/2000.

  1433-7851/01/4007-1163 $ 17.50+.50/0

has inspired and encouraged electrochemists to ask similar questions about the microscopic structure of the metal/electrolyte interface, about the influence of the surface structure on electrochemical reactions, and about the electronic and vibronic properties of adsorbates and their change with potential, to mention just a few. To find answers to such questions, however, required new routes involving new techniques, new types of electrodes, and new theoretical concepts.[12]

2. The Experimental Basis of an Electrochemical Surface Science

Among the various requirements necessary to derive a microscopic picture of electrochemical processes, the following four in my opinion were the most crucial ones:[13] 1) new techniques, 2) single-crystal surfaces with fully defined structures, 3) linking electrochemistry with UHV methods (ex situ approaches), and 4) new theoretical methods.

2.1. New Experimental Techniques

New experimental techniques were required that were able to provide information on a molecular basis but were applicable in situ. Quite obviously, these were optical spectroscopies. Reflectance spectroscopy in the visible and near-UV range, particularly electroreflectance, was among the first of the so-called nontraditional methods to address questions of the optical and electronic properties of adsorbates and thin metal or oxide overlayers.[14] Later, this method was used to derive surface structure information by determining rotational anisotropies at normal incidence from linearly polarized light or involving surface band-structure effects.[15] Then came surface-enhanced Raman spectroscopy, with which vibronic information became accessible.[16] With the development of optical thin-layer cells for infrared studies a major barrier was shifted:[17] In the end, almost the whole spectrum—from infrared to X-rays—became accessible for in situ studies. In situ IR spectroscopy began to yield invaluable information about reaction intermediates,[18] whereas in situ X-ray diffraction and absorption provided structural information of astounding precision and detail.[19–22] Other nontraditional in situ techniques have joined in, such as the quartz-crystal microbalance for monitoring mass changes in the submonolayer range,[23] spectroscopies based on nonlinear optics, such as second harmonic generation (SHG)[24, 25] or sum-frequency generation (SFG),[26] neutron scattering,[27] and even NMR spectroscopy.[28] A tremendous advance, however, came about with the scanning tunneling microscope, which soon after its invention for surface studies under UHV conditions[29, 30] was adopted to electrochemical needs.[31–33] This technique, which will play a dominant role in the studies described below, allows imaging of electrode surfaces in situ, in real space, and with atomic-scale resolution.

2.2. Single-Crystal Surfaces

For a detailed understanding of surface processes, the use of single-crystal electrodes with structurally well-characterized surfaces is highly desirable. Polycrystalline surfaces, routinely employed in the early days of electrochemical surface studies, are far too complicated for a reliable interpretation on an atomic level. Single-crystal surfaces need to be prepared and their structure characterized, which is by no means a trivial task for electrochemists. Since the classic method of preparing single-crystal surfaces involves sputtering and annealing of the crystal in a UHV chamber, the first systematic studies with single-crystal electrodes addressing the influence of the surface structure were performed with UHV-prepared samples in an apparatus that had a closed-transfer system between the electrochemical cell and UHV chamber.[34–37] In parallel, single-crystal electrodes were prepared simply by mechanical and chemical or electrochemical polishing but without structural characterization; the quality of the data in retrospect varied from satisfactorily to unacceptable.

A major breakthrough was achieved when Clavilier et al. demonstrated that high-quality single-crystal platinum surfaces could be prepared simply with a Bunsen burner.[38, 39] This so-called flame annealing, which was subsequently shown to work also for gold and silver,[40] consisted of heating the crystal in the flame of a Bunsen burner for several seconds or minutes before it was quenched in ultrapure water and transferred to the electrochemical cell with a droplet of water

Dieter M. Kolb, born in 1942 in Amberg (Germany), studied physics at the Technical University, Munich. After postgraduate research with H. Gerischer, he received his doctorate from Munich in 1969. During 1969 – 71, he was a postdoctoral fellow at the Bell Laboratories, Murray Hill, studying the optical properties of electrode surfaces by reflectance spectroscopy. From 1971 until 1990, he was a senior scientist and head of a working group at the Fritz Haber Institute of the Max Planck Society in Berlin, where he pursued a surface-science approach to interfacial electrochemistry. In 1984, he was appointed Apl. Professor at the Freie Universität Berlin and, in 1990, appointed full professor at the Universität Ulm. His main research interest is electrochemical surface science, with emphasis on metal deposition, electrocatalysis, and electrochemical nanostructuring. He has received awards, among others, from the Deutsche Bunsengesellschaft, the International Society of Electrochemistry, and the American Electrochemical Society.

adhering to the polished surface. The latter was crucial in protecting the surface from airborne contaminants. This procedure was later modified, when it became evident that the heat shock during immersion of the still-hot crystal into water was detrimental to both surface structure and bulk crystallinity.[41] The crystals were then allowed to cool to almost room temperature in air (gold) or in an inert (N_2 or Ar for silver) or reducing (H_2 or CO for platinum) atmosphere, which yielded large, atomically flat terraces.[42, 43] In case of the three low-index faces of gold, flame annealing with subsequent slow cooling led to reconstructed surfaces, very much like those obtained in UHV by sputtering and annealing.[44, 45] Two more observations helped to make single-crystal electrochemistry an easier game to play (at least with gold). 1) Thin gold films (about 200 nm thick) evaporated onto a special heat-resistant glass can be flame annealed to yield fairly good (111) surfaces. These are relatively cheap substitutes of massive Au(111) single crystals, which can be disposed of after use. 2) Besides thermal annealing, there is an electrochemical (room temperature) annealing to restore single crystallinity of a gold surface which had been maltreated, for example by alloy formation and dissolution.[46] The effect is based on an anion-enhanced surface mobility of gold atoms and operates best in solutions containing specifically adsorbing anions, such as chloride, at potentials clearly positive of the potential of zero charge (pzc).[47, 48]

2.3. Ex Situ Approaches

Historically, the ex situ approach to electrochemical surface science was extremely important for the development of this field. In the 1970s, there were no structure-sensitive techniques available for in situ studies. Hence, electrochemists adopted UHV techniques, particularly low-energy electron diffraction (LEED), to check the quality of UHV-prepared single-crystal surfaces before and after electrochemical treatment.[49] UHV studies were then extended to strongly bound adsorbates, such as iodide,[50] metal,[51] or oxide overlayers;[52] systems that were believed to undergo little or no changes after transfer into the UHV. Here, an important step forward was achieved by W. N. Hansen, when he showed that electrodes could be emersed with their electric double layer intact (see Section 3).[53] The studies of emersed electrodes that followed and, to a lesser extent, the double-layer simulation studies (an attempt to compose the electric double layer under UHV conditions by adsorbing, for example, water and metal ions[54]) yielded a wealth of information about bare and adsorbate-covered electrodes. Examples are the study of surface reconstruction[55] or ordered adsorption occurring during metal-monolayer formation.[37, 56]

2.4. Modern Theoretical Concepts and Methods

The fourth point that contributed in a significant way to the development of modern interfacial electrochemistry was the adoption of theoretical concepts and methods from solid-state physics or statistical mechanics, among others. This was particularly important for a better understanding of the electric double layer or of the solvent structure near a charged wall in general. A good example is the "jellium" model for the description of metal surfaces, which was adopted by electrochemists to account for the influence of the metal side on the double-layer capacity.[57, 58] Such an influence was safely established from measurements with solid electrodes but could not be satisfactorily explained by the earlier double-layer models, which only accounted for contributions from ions and water dipoles to the double-layer capacity. Other important results came from computer simulations of the electric double layer, which yielded new information about the spatial distribution of ions and water molecules near the electrode surface. One example thereof will be given in Section 3.1.

In the following, selected examples of electrochemical surface-science studies will be presented, to demonstrate the type of problems currently addressed in many electrochemical laboratories and, particularly, in the Department of Electrochemistry at the University of Ulm.

3. The Electric Double Layer

3.1. Double-Layer Models

The electric double layer is a central issue in electrochemistry. It is the place of electron and ion transfer, and the region where chemical and electric potentials are different from the neighboring phases, electrode and electrolyte. For generations of electrochemistry students, the electric double layer of a metal/electrolyte interface was described by a plate condenser of molecular dimensions (Figure 1): One plate is the metal surface with its excess charge, the other is formed by solvated ions at closest approach.[9] Experimental values for the double-layer capacities of, say, silver single-crystal electrodes in 0.1 M solutions range between 20 and 50 $\mu F\,cm^{-2}$ with a pronounced maximum around the potential of zero charge (pzc). Assuming a "plate distance" of about 0.3 nm, the radius of a solvated ion, we obtain a relative dielectric constant of roughly 5–10 for the interfacial water, namely, for water molecules in a strong electric field. The solvated ions that form the outer Helmholtz plane (OHP, see Figure 1) and that are held in position by purely electrostatic forces are termed "nonspecifically adsorbed". These are mainly solvated cations or anions with a strong solvation shell, such as fluoride. Most anions however (with their inherently weaker solvation shell) give away part of that solvation shell when entering the double layer to form a chemical bond with the electrode surface. These ions are termed "specifically adsorbed" and their centers form the inner Helmholtz plane (IHP, see Figure 1). Because the chemical interaction between (specifically adsorbed) anions and electrode surface causes more charge to be accumulated at the surface than required by electrostatics, countercharge (cations, in this case) is brought into the double layer for charge compensation. Consequently, while a linear potential drop is generally assumed for nonspecifically adsorbing ions, as for a plate condensor, specific adsorption of ions causes a steeper potential gradient (close to

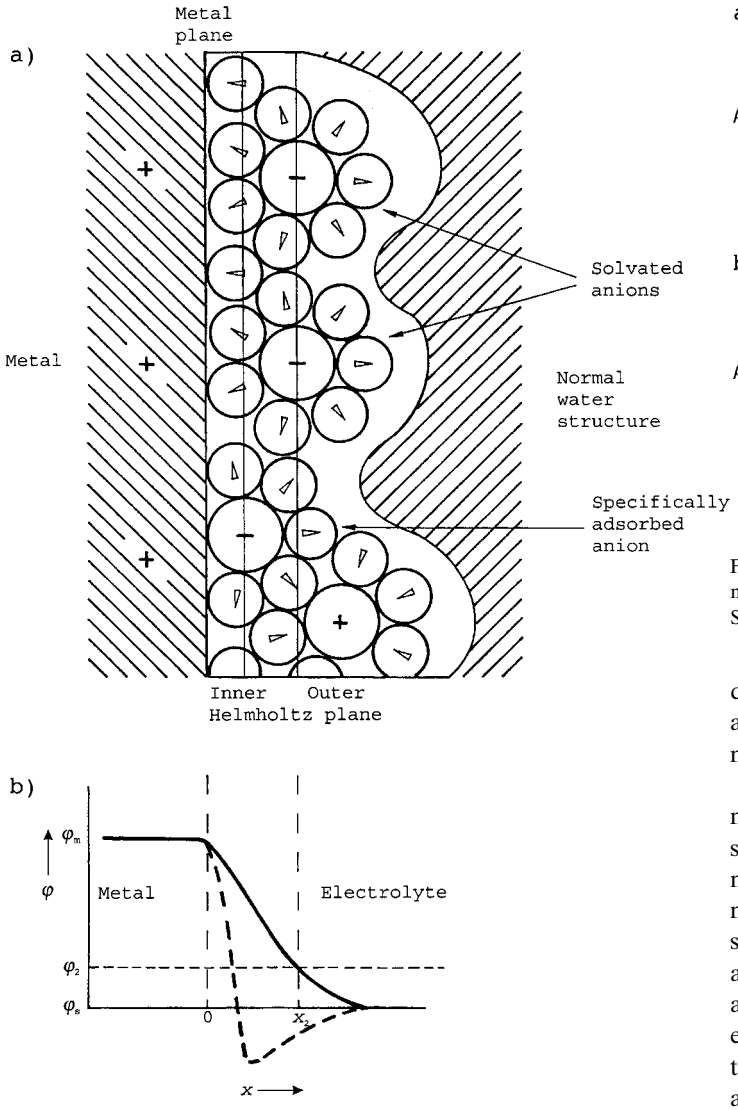

Figure 1. a) Model of the metal/electrolyte interface. b) Potential distribution across the electrochemical interface for a purely electrostatic interaction between solvated ions and the metallic surface (——) and for the case of specifically adsorbing anions (- - - -).

the surface) and an "overshoot" of the potential with respect to the solution value before the latter is reached.

While this simple double-layer model works surprisingly well in that it can explain most of the experimental observations, a more detailed (and realistic) picture which, for example, takes the discreteness of a charge into account, is clearly desirable. Considerable advancement had been achieved during the last two decades, mainly by means of computer simulations.[59, 60] An example is given in Figure 2, where for a 2.2 molal NaCl solution the densities of Na^+ and Cl^- as a function of distance z from the surface of a charged metal is shown, the latter being either positively or negatively charged.[61] An oscillating density profile for $z < 10$ Å is clearly seen for both ions, similar to that for water (for example, its oxygen density), which reflects the "layering effect" found in liquids near a wall.[62] We also see the closer approach of the anion due to specific adsorption. The very pronounced first density maximum for Na^+ and Cl^- allow

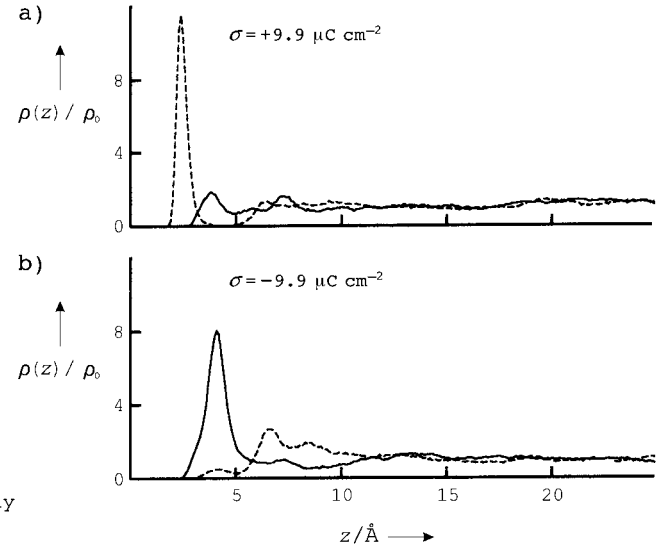

Figure 2. Normalized ion densities $\rho(z)/\rho_0$ for Na^+ (——) and Cl^- (- - - -) near a positively (a) and a negatively (b) charged wall ($z = 0$) in 2.2 M NaCl. Surface charges are $+9.9$ and $-9.9\ \mu C\,cm^{-2}$, respectively. From ref. [61].

definition of planes which correspond directly to the outer and inner Helmholtz planes of the classical double-layer model (Figure 1).

A longstanding question in relation to the double-layer models concerns the electric field strength near metal surfaces. Applying an electrode potential 1 V positive or negative of the pzc, which according to our plate condenser model corresponds to a potential drop of 1 V across 0.3 nm, should give rise to extremely high electric field strengths of about $3 \times 10^7\ V\,cm^{-1}$. With such large numbers, interesting and easily accessible experimental observations, such as electrochromism, were expected. In fact, the contrary seems to be the case. Electroreflectance studies of dye molecules adsorbed at gold electrodes led to estimated values which were about two orders of magnitude lower than the above mentioned value ($\approx 10^5\ V\,cm^{-1}$[63]). An obvious problem arises from the extremely small distance over which the high field strength exists. Classical dye molecules, which absorb in the visible region and hence are easily studied by in situ optical spectroscopies, are too large to be accommodated inside the double layer. Small molecules like CO have their absorption band in the far-UV range and hence are difficult to study in situ. There are, however, two pieces of information that point towards the high field expected near the surface of a metal electrode. These originate from surface-state spectroscopy and from ex situ ESCA measurements (ESCA = electron spectroscopy for chemical analysis).

3.2. Surface-State Spectroscopy

For gold and silver single-crystal electrodes in contact with an aqueous solution, there exist the very same electronic surface states that are found for such surfaces in UHV.[64–66] It has been shown that the energetic position of surface states at metal/electrolyte interfaces relative to the bulk states of the metal depends on the electrode potential. Because surface

states penetrate significantly into the electric double layer—their "center of gravity" being assumed to be roughly 0.1 nm outside the metal, if one defines the metal surface by the location of the surface-atom cores—these states feel the potential drop across the double layer.[67] Hence, the energy of the surface states changes differently than that of the bulk states when the electrode potential is altered. For example, when we change the electrode potential by 1 V in a positive (negative) direction, then the bulk states of the metal, including its Fermi level, are shifted exactly by 1 eV to higher (lower) electron binding energies; the energy shift of the surface states would be only a fraction of 1 eV depending on the fraction of the total potential drop that exists at the position of the surface states. With the total potential drop occurring, for example, over 0.3 nm and the surface states being located 0.1 nm away from the metal surface, the potential-induced shift in energy for surface states would only be ⅔ of that for the bulk states (with reference to the potential in solution). For all three low-index faces of gold and silver, optical transitions from occupied bulk states into empty surface states have been observed. The transition energy $\hbar\omega$ would be expected to change with potential E according to $\delta\hbar\omega/\delta E \approx 0.3\ \mathrm{eV\,V^{-1}}$, if the above described situation would hold and if a linear potential drop across the 0.3 nm region can be assumed. An experimental result for Au(100) in 0.5 M $NaClO_4$ is given in Figure 3, where the photon energy for an

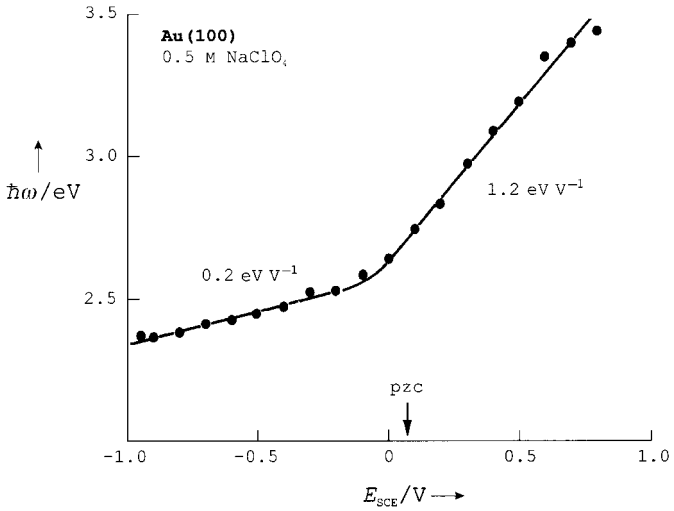

Figure 3. Optical excitation energy $\hbar\omega$ for the transition from bulk d-states into empty surface state B of Au(100) in 0.5 M $NaClO_4$ as a function of electrode potential. The potential of zero charge (pzc) is indicated by an arrow. From ref. [66].

optical transition from bulk d-states into the empty surface state B at $\overline{X}$ of the surface Brillouin zone is plotted as a function of electrode potential.[66] For potentials negative of the pzc, where solvated (nonspecifically adsorbed) cations form the double layer, a shift of 0.2 $\mathrm{eV\,V^{-1}}$ has been measured, which is consistent with the simple plate-condensor model and a linear potential drop across the double layer. However, for potentials positive of the pzc, where specifically adsorbing anions set up an inner Helmholtz plane, a surprisingly large shift of 1.2 $\mathrm{eV\,V^{-1}}$ is observed. This value points towards a high potential gradient near the metal surface that is felt by the surface states and that should be a result of the discrete nature of the ionic double-layer charge.

3.3. Ex Situ ESCA Measurements

Information about the potential gradient near the metal surface can also be obtained from measurements of the electrochemical shift for electron binding energies in ESCA spectra.[68] This, of course, requires the withdrawal of the metal electrode with its electric double layer from the electrochemical environment and transfer to an UHV chamber. The emersion of electrodes from solution with its inherent loss of potential control and solution phase has been critically viewed by many electrochemists as far as compatibility with in situ information was concerned. However, in a number of rather thorough studies, it was shown that for a limited number of systems (which did include gold electrodes) the electrode can be emersed with its double layer essentially intact. We shall return to this point shortly. As we discussed above for surface states, any adsorbate, atom, ion, or molecule that is located inside the double layer will feel an electrostatic potential that is different from that for the bulk electronic states. In photoelectron spectroscopy, all electron binding energies, which includes those for adsorbates, are measured relative to the Fermi level of the substrate.[69] Hence, the adsorbate's electronic states shift in energy with electrode potential (electrochemical shift) and, with our simple double-layer model, we can foresee the following two borderline cases: 1) no electrochemical shift, when the adsorbate is strongly electronically coupled to the substrate, and 2) an electrochemical shift of 1 $\mathrm{eV\,V^{-1}}$, when the adsorbate resides at the outer Helmholtz plane and its electronic levels linked to those in solution. In several studies, electrochemical shifts of the order of 1 $\mathrm{eV\,V^{-1}}$ have been reported, even for strongly adsorbed molecules,[70–73] which again suggests potential gradients near metal surfaces that are higher than those expected for our plate-condensor model. A remarkable observation is shown in Figure 4, where the electrochemical shifts for sulfate and water on Au(111) are reproduced.[74] Much to our surprise, we found two clearly different shifts for the components of one and the same molecule, namely sulfate: Whereas for the S-$2p_{3/2}$ level an shift of 1.3 $\mathrm{eV\,V^{-1}}$ was observed, only 0.4 $\mathrm{eV\,V^{-1}}$ was found for the O-1s level of the sulfate oxygen atom. It thus appears that the different atoms of sulfate feel different electrostatic potentials, which supports the idea of using small adsorbed molecules for sensing the spatial variation of the double-layer potential. Assuming the sulfate anion sits on the Au(111) surface with three oxygen atoms directed towards it, we expect a larger electrochemical shift for the more remote sulfur atom than for these three oxygen atoms, which is indeed the case (the fourth oxygen atom, of course, would be even further away from the metal surface and should show the largest electrochemical shift; however, its contribution may be masked by those from the three equivalent oxygen atoms close to the metal). Such simple geometric considerations may be too naive an approach to the microscopic structure of the

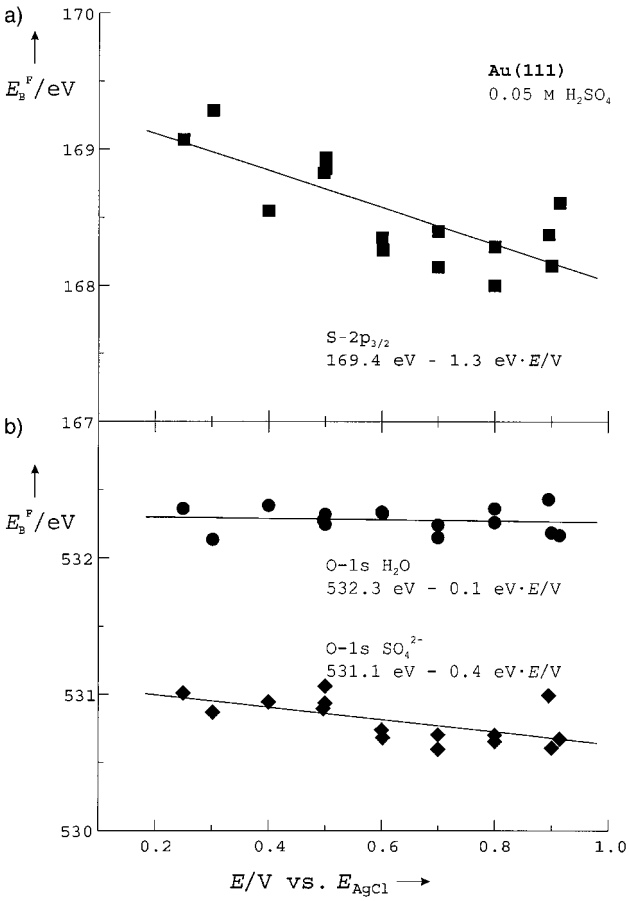

Figure 4. Dependence of electron binding energies E_B^F on the emersion potential E ("electrochemical" shift) for Au(111) in 0.05 M H_2SO_4. a) S-2p$_{3/2}$ level of sulfate; b) O-1s level of sulfate (◆) and of H_2O (●). From ref. [74].

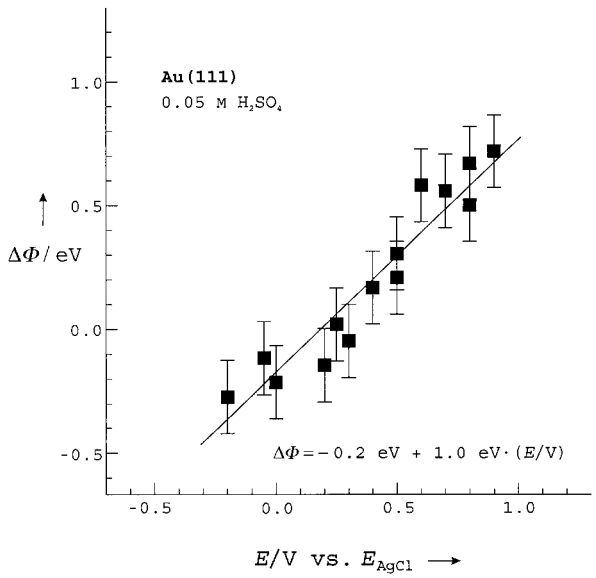

Figure 5. Changes in the work function $\Delta\Phi$ of an emersed Au(111) electrode as a function of emersion potential; $\Delta\Phi = 0$ is referenced to the work function of a UHV prepared, bare Au(111)-$(22 \times \sqrt{3})$ surface. From ref. [74].

electric double layer. What remains, however, is an interesting experimental observation that calls for a systematic study of electrochemical shifts in ESCA and for theoretical support. Also noteworthy is the vanishingly small electrochemical shift of the O-1s signal that originates from water rather than from sulfate (Figure 4). This assignment can be unequivocally made from the *chemical* shift of O-1s. It implies that this water is bound to the metal surface.

As mentioned above, ex situ experiments are only meaningful for electrochemists if the electrode can be emersed with its electric double layer unchanged. A crucial test in this respect comes from work function measurements with emersed electrodes as a means of determining the potential drop across the double layer in the emersed state. As has been frequently stated, the work function and electrode potential represent one-and-the-same quantity, namely the electrochemical potential of the electrons in the metal. Hence, a 1:1 correlation is expected for the work function of emersed electrodes as a function of emersion potential if the potential drop across the double layer is retained during and after withdrawal of the electrode from the electrochemical cell. For gold electrodes, such a 1:1 relation has been found in numerous studies.[75, 76] Equally important were deviations from the ideal 1:1 behavior, from which we learnt about double layer collapses after emersion and their origins.[68, 77] Figure 5 shows the result from a recent study of Au(111) in 0.05 M H_2SO_4, which again demonstrates the 1:1 correlation between work function and emersion potential.[74] The work function was determined from ESCA spectra by the cut-off of the secondary electron emission and referenced to that of the bare, reconstructed Au(111) surface after sputtering and annealing in the UHV chamber and before immersion into the electrolyte. Taking $\Phi = 5.3$ eV for bare, reconstructed Au(111) from literature,[78] the $\Delta\Phi$ axis of Figure 5 can be transformed into an absolute Φ-scale, which allows one to calculate the absolute electrode potential, namely, the potential of the normal hydrogen electrode (NHE) referenced to vacuum (in other words, the work function of NHE). With $E_{NHE} = -0.2$ V versus Ag/AgCl, we obtain a work function value of about 4.8 – 4.9 eV for the NHE. This number appears somewhat high but still falls into the 4.7 – 4.8 eV range obtained by similar methods[76, 79] and by in situ optical spectroscopy.[80] It is clearly at variance with the IUPAC-recommended value of 4.44 eV[81] and adds to the on-going controversy between the two schools of thought.

4. Surface Reconstruction

In order to derive a microscopic picture of surface processes such as adsorption or deposition, single-crystal material is generally used, for which the surface structure is believed to be precisely known. This tacitly assumes that the atoms at the surface retain their bulk positions and hence the surface structure can be derived directly from the well-known bulk structure. Although most metal surfaces fulfill this expectation, some do not. The reason for the latter cases is that the highly asymmetrical environment of the surface atoms, due to missing neighbors, can lead to a rearrangement in the top layer. Typically, atoms at surfaces tend to acquire a more densely packed structure because of an increased electron

density between the surface atom cores.[82] Such a rearrangement of surface atoms, which often involves local bond breaking and a change in surface symmetry, is called surface reconstruction.[83, 84] Typical examples of such an effect are the bare low-index surfaces of gold which all reconstruct in order to reduce the surface energy. An eye-catching structural change due to surface reconstruction is seen with Au(100), which reconstructs into a hexagonal close-packed surface (hex structure) when prepared under UHV conditions.[85] While for the bare surface the reconstructed state is energetically more favorable than the unreconstructed (1×1) state, the opposite is normally the case for adsorbate-covered surfaces, as adsorption is energetically more favorable on the less dense, unreconstructed surface.[86] Because of an activation barrier for reconstruction, removal of the adlayer that was responsible for lifting of the reconstruction does not bring back the reconstructed surface; the latter process normally requires heating of the sample.

For gold single-crystal electrodes in contact with an aqueous solution, the very same reconstruction phenomena as for surfaces in UHV were observed.[87, 88] Flame-annealed gold electrodes, to begin with, reconstruct in the same way as in UHV, namely Au(111)-$(22 \times \sqrt{3})$, Au(100)-(hex), and Au(110)-(1×2) or -(1×3), and the reconstruction can be retained upon immersion into the electrolyte, provided certain precautions are met. Since specific adsorption of anions lifts the reconstruction, it is absolutely essential to immerse the reconstructed electrode under control of the potential, clearly negative of the pzc.[44, 45]

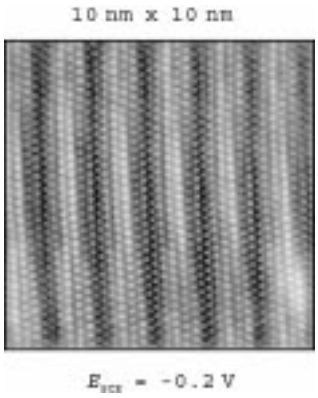

Figure 6. STM image of a reconstructed Au(100) electrode in 0.1 M H_2SO_4 showing the hexagonal arrangement of the surface atoms. The surface was prepared by flame annealing. From ref. [88].

Figure 6 shows the STM image of a freshly prepared (flame-annealed), reconstructed Au(100) surface in 0.05 M H_2SO_4 at $E_{SCE} = -0.2$ V (E_{SCE} = potential versus a saturated calomel electrode). The hexagonal arrangement of the surface atoms is clearly seen, together with the so-called reconstruction rows (they run vertically in Figure 6), which arise from the fact that the (hex)-structured surface is slightly buckled, since it is no longer congruent with the underlying second layer. The corrugation length of the reconstruction rows is 1.45 nm; its height is about 0.05 nm. These rows are a convenient sign of a (100) surface to be reconstructed in all those cases where atomic resolution is not obtained and, hence, where the hexagonal arrangement of the surface atoms cannot be seen directly. Well-prepared reconstructed Au(100) surfaces show large (hex)-structured domains with the reconstruction rows being aligned along monoatomic high steps. Very often a terrace is covered by a single domain.[88, 89]

Since the optical as well as the electrochemical properties of reconstructed and unreconstructed Au(100) surfaces are distinctly different, the existence of Au(100)-(hex) in an electrochemical environment has been shown well before the STM entered the scene.[44, 90] In Figure 7, the electroreflectance (ER) spectra of reconstructed and unreconstructed

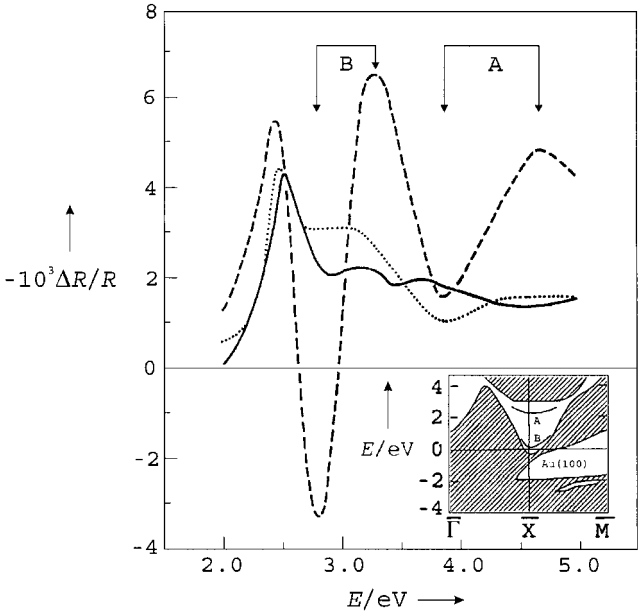

Figure 7. Normal-incidence electroreflectance spectra of Au(100)-(hex) (——), Au(100)-(1×1) (- - - -), and Au(111) (••••) in 0.01 M $HClO_4$. Inset: Surface band structure of Au(100)-(1×1) with surface states A and B. From refs. [15, 44].

Au(100) in 0.01 M $HClO_4$ are shown and that of Au(111) in the same electrolyte for comparison. Note that in ER spectroscopy, the normalized reflectance change $\Delta R/R$ with a change of electrode potential is measured. While the reconstructed Au(100)-(hex) surface exhibits an ER spectrum very similar to that of Au(111), the ER spectrum of the unreconstructed Au(100)-(1×1) differs vastly. The pronounced, derivative-like structures, labeled A and B in Figure 7, originate from optical transitions into the empty surface states A and B that are found at $\overline{X}$ of the surface Brillouin zone (see Figure 7 inset). The complete absence of the surface state features A and B (Figure 7) in the ER spectrum of Au(100)-(hex) leads, for certain wavelengths, to a pronounced difference in the optical response of reconstructed and unreconstructed Au(100) that has been utilized to study the kinetics of the (hex) $\rightarrow (1 \times 1)$ structural transition.[90] Furthermore, the electrochemical properties of (hex) and (1×1) surfaces differ markedly, mainly because the pzc values of both surfaces differ by about 220 mV. This is demonstrated in Figure 8. We recall that for dilute solutions—in this case 0.01 M $HClO_4$—the double-layer capacity has a pronounced minimum at the pzc due to the contribution from the diffuse part of the double layer.[1–3] Starting the measurement with a freshly flame-annealed, namely reconstructed, Au(100) electrode, a pzc of about +0.30 V versus SCE is observed, which is very close to that of Au(111). This is not unexpected as both surfaces have a hexagonal close-packed structure. Systematic studies have revealed that the specific

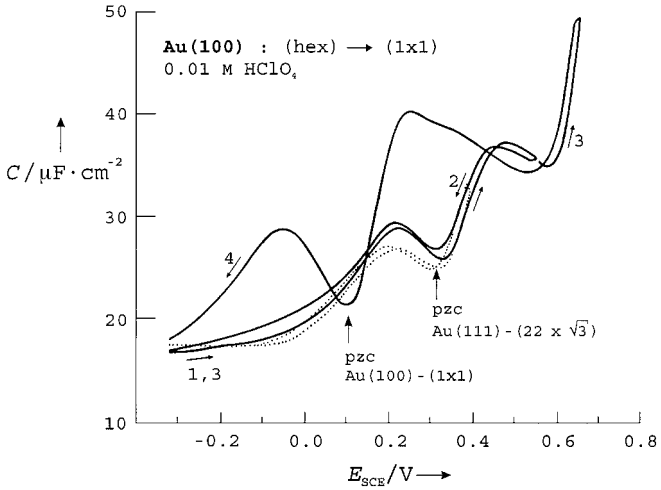

Figure 8. Double-layer capacity C as a function of electrode potential for Au(100)-(hex) in 0.01M $HClO_4$ with a transition from (hex) to (1×1). Numbers refer to the scan sequence. The capacity curve for Au(111)-$(22\times\sqrt{3})$ is shown for comparison (••••). From refs. [44, 90].

adsorption of anions lifts reconstruction and the gold surface acquires the (1×1) structure. The transition potential depends on the type of anion and it shifts in negative direction with increasing strength of chemisorption.[45] For 0.01M $HClO_4$, the (hex) $\rightarrow(1\times1)$ transition occurs around $+0.6$ V versus SCE. When the potential scan under the conditions shown in Figure 8 exceeds $+0.6$ V (scan 3), the reconstruction is lifted and the well-known capacity curve for the unreconstructed Au(100) emerges with its pzc at about $+0.08$ V versus SCE. The shift in pzc by 220 mV, which is connected with the (hex) $\rightarrow$(1x1) transition, reflects a corresponding change of 0.22 eV in work function to lower values. This sudden shift in pzc with lifting of the (hex) reconstruction requires additional charging of the electrode surface to maintain the applied potential during the structural transition, and this gives rise to a pronounced current peak. This is shown in Figure 9 for Au(100) in 0.1M H_2SO_4, where reconstruction is lifted already around $+0.36$ V (the exact value depending somewhat on the scan rate). This current peak has turned out to be a convenient

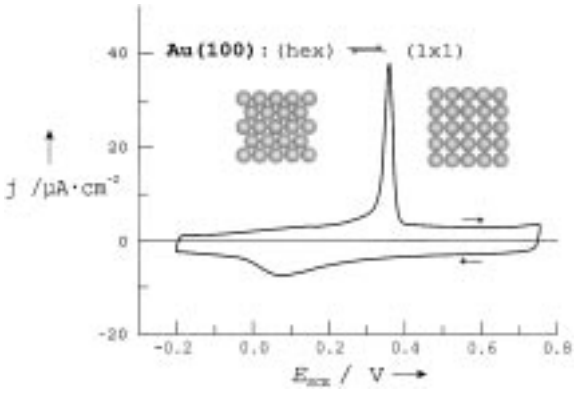

Figure 9. Cyclic current–potential curve for Au(100) in 0.1M H_2SO_4 starting at -0.2 V with a freshly prepared reconstructed surface. Scan rate: 50 mV s^{-1}. Lifting the (hex) reconstruction during the positive scan is seen by a pronounced current peak at $+0.36$ V. The subsequent scan in negative direction reflects the electrochemical behavior of Au(100)-(1×1). From ref. [88].

and easily accessible indicator for reconstruction: The peak potential is a measure for the stability range of the (hex) structure; the charge under the peak is a measure for the fraction of the electrode surface that is reconstructed.[91]

A very remarkable observation can be made at the gold/electrolyte interface, which is not possible for UHV. Applying a negative potential (with respect to the pzc) to the unreconstructed Au(100) surface brings back the (hex) reconstruction.[92] This *potential-induced* reconstruction has been observed for all three low-index gold faces. Under UHV conditions, the bare unreconstructed gold surfaces are in a metastable state; reconstruction of the uncharged surface is prevented at room temperature by an activation barrier. However, application of an electrode potential sufficiently negative of the pzc to the unreconstructed Au(100) surface will not only free the surface from anions but also lower the activation barrier to such an extent that reconstruction occurs within seconds or minutes, even at room temperature. This phenomenon has far-reaching consequences for electrochemical studies with gold single-crystal electrodes: The surface structure of the electrode becomes a function of potential! Only at potentials sufficiently positive of the pzc is the structure of the single-crystal surface that expected from the bulk structure. At negative potentials, however, a potential-induced reconstruction sets in to transform, for example, an Au(100) surface into one that is Au(111)-like. From the cyclic voltammogram of Figure 9, we can conclude that lifting the reconstruction is a much faster process than the $(1\times1)\rightarrow$(hex) transition at negative potentials. Therefore, the potential scan in the negative direction (Figure 9), from $+0.75$ to -0.2 V, reflects in essence the double-layer capacity of Au(100)-(1×1). For the much faster $(1\times1)\rightarrow$(rec.) transition of Au(111), potential-induced reconstruction spreads within a matter of seconds, which makes it very difficult, although not impossible, to perform experiments in the potential range negative of the pzc with an unreconstructed Au(111) surface. Since both structural transitions, potential-induced reconstruction and anion-induced lifting, require surface imperfections as nucleation centers to start the transition, these reactions can be suppressed to a great extent by working with surfaces as free of defects as possible. Electochemical annealing has been shown to be important for protecting unreconstructed surfaces against potential-induced reconstruction.[89, 93a]

Finally, a few words should be said about the topography of the unreconstructed Au(100) surface. Because the (hex) structure has a packing density about 25% higher than that of Au(100)-(1×1), gold atoms are expelled from the surface during the (hex) $\rightarrow(1\times1)$ transition. They coalesce and form monoatomic high islands of gold, which cover about one quarter of the surface. Such a surface is shown in Figure 10. I mention in passing that these islands undergo substantial Ostwald ripening after their formation, the rate of which depends significantly on the electrode potential (electrochemical annealing), and which helps to improve the smoothness of the surface. Nevertheless, it should remain borne in mind, that lifting of the reconstruction inevitably leads to a defect-rich surface, as the rims of the monoatomic high islands constitute surface imperfections.

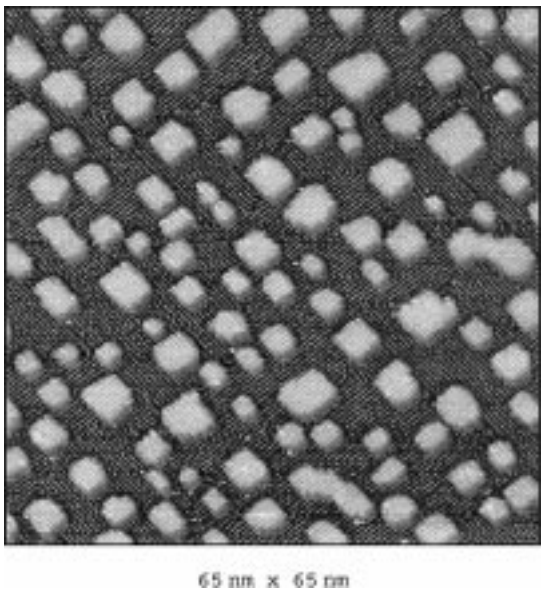

Figure 10. STM image of an unreconstructed Au(100) surface in 0.1M H_2SO_4 at +0.35 V versus SCE, recorded shortly after lifting of the (hex) reconstruction. The surface is strewn with monoatomic high islands of Au. The line pattern arises from ordered sulfate adsorption. From ref. [93b].

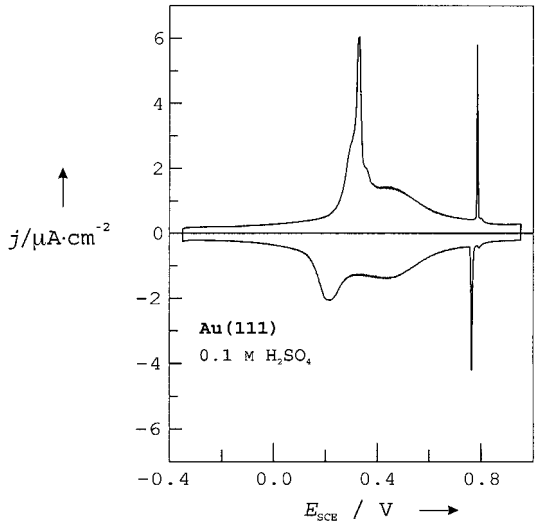

Figure 11. Cyclic current–potential curve for Au(111) in 0.1M H_2SO_4 starting with a freshly prepared reconstructed surface at −0.35 V. Scan rate: 10 mV s^{-1}.

5. The Study of Adsorbates

Since many electrochemical reactions involve an adsorption step at some point, the study of adsorbates or adlayers is of particular interest for a mechanistic interpretation. However, adsorbed species often show extensive surface diffusion at room temperature and, hence, escape detection by the STM. In order to be able to image individual atoms, ions, or molecules on surfaces, the species under study has to be immobilized. This is normally achieved either by forcing the adsorbed species into a densely packed monolayer or allowing long-range order between the adspecies to lead to ordered adsorption, where lateral forces keep the entity in place. Ordered adlayers have become a favorite playground for STM studies, where important structure information combines with the fascination of "seeing" single atoms or molecules.[94]

The formation of ordered adlayers, namely of adlayers where the atoms or molecules are arranged on the surface in a regular pattern, is often accompanied in cyclic voltammograms by a very pronounced current spike: This means the ordered adlayer is formed within a very narrow potential region, which is indicative of a first-order phase transition. A typical example is given in Figure 11, where the cyclic voltammogram for Au(111) in a sulfuric acid solution is shown. Besides the pronounced current peak at +0.3 V versus SCE on the potential scan in positive direction, which is due to lifting of the $(22 \times \sqrt{3})$ reconstruction, a pair of extremely narrow current spikes is noted around +0.73 V versus SCE, which was assigned to a phase transition in the anionic (sulfate) adlayer.[95] The latter was indeed observed by structure-sensitive methods, such as in situ X-ray diffraction at grazing incidence[96] and, in particular, the STM. Figure 12 shows an STM image of Au(111) in 0.1M H_2SO_4, where the potential was stepped during imaging from +0.65 to +0.80 V versus SCE (see arrow in Figure 12). At the former potential, the adsorbed sulfate (or bisulfate) ions are mobile and hence cannot be imaged with the STM. Instead, the surface atoms of the gold substrate are clearly visible and provide an internal calibration for lateral distances and crystallographic orientations. With the potential step to +0.80 V versus SCE, an ordered sulfate adlayer is formed instantaneously with, after LEED terminology, a $(\sqrt{3} \times \sqrt{7})$R19.1° superstructure. Although the image of the adlayer depends somewhat on the tunnel voltage, all research groups so far have unanimously reported two different reflexes, a main and a side maximum per unit cell, each corresponding to 0.2 monolayers (ML). Since the coverage of sulfate has been determined to 0.2 ML by chronocoulometric measurements,[97] it had to be concluded that the main and side maxima belong to two different chemical species. It seems currently accepted that the side maximum corresponds to coadsorbed hydronium ions, while

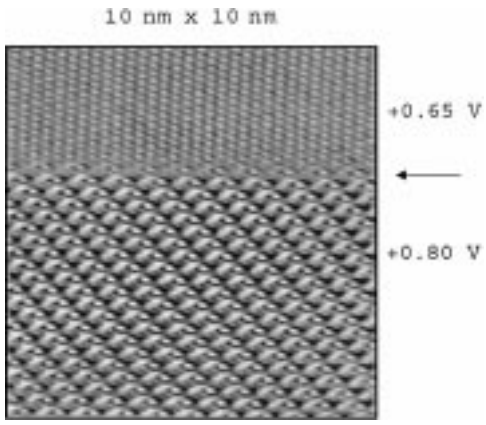

Figure 12. High-resolution STM image of Au(111) in 0.1M H_2SO_4. The upper part shows the Au(111) surface, atomically resolved, at +0.65 V versus SCE; the lower part shows the ordered adlayer of sulfate, formed by a potential step to +0.80 V versus SCE.

the main reflexes are due to sulfate (or bisulfate). In the image of Figure 12, the main (sulfate) reflexes are rather broad with a lengthy shape, whereas the side maxima appear as small round spots which—interestingly enough—are exactly at positions of the gold atoms. This would imply that the coadsorbed hydronium ions occupy on-top positions, if the assignment of the side maxima is correct. I mention in passing that, due to thermal drift and inaccuracies in scanner calibrations, an internal standard for distances is almost mandatory for the safe determination of adsorbate structures from STM images. The most convenient standard is, naturally, the bare metal substrate, as demonstrated in Figure 12.

Another example of an ordered adlayer, formed out of specifically adsorbing anions, is given in Figure 13, which may also demonstrate the aesthetic of STM images. It shows a layer of tetrachloropalladate anions on Au(110) at $+0.61$ V versus SCE.[98] Besides the formation of rows of adions, which

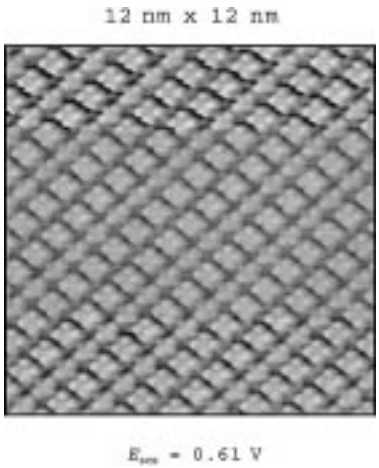

Figure 13. High-resolution STM image of an ordered adlayer of $[PdCl_4]^{2-}$ on Au(110) in 0.1 M H_2SO_4 + 1 mM H_2PdCl_4. From ref. [98].

is not unexpected for a substrate with two-fold symmetry, it is noteworthy that flat-lying $[PdCl_4]^{2-}$ ions are imaged as little pinwheels, a center reflex being surrounded by four reflexes arranged in a square. Considering the well-known square-planar structure of $[PdCl_4]^{2-}$, it appears that the fine structure in the image of each anion shows its atomic components, namely the palladium atom in the center and the four surrounding chloro ligands. High-resolution images like the one in Figure 13 nourish the hope that individual components of complex molecules—functional groups or even atoms—will be seen by STM.[99, 100] This perspective seems particularly interesting for biological molecules.

A second group of ordered adlayers, which has been intensively studied by STM, are the self-assembled monolayers (SAMs).[101] These are formed by molecules with a functional group that interacts strongly with the substrate. A classical system is alkanethiols on gold, particularly on Au(111), where the strong interaction between gold and sulfur leads to a stable and ordered adlayer upon mere immersion of the gold substrate into a thiol solution. Introduction of functional groups at the other end of the thiol allows for a chemical modification of electrode surfaces, which bears great potential for future applications, for example in the areas of sensors or molecular electronics. Here again, STM has contributed significantly to the understanding of the adlayer properties by yielding detailed structural information. While most of the STM studies of alkanethiol SAMs so far were performed in UHV or in air, the number of investigations of SAM-covered gold surfaces in an electrochemical environment is steadily increasing.[102] Although the structure of SAMs in many cases is the same in situ and ex situ, there are distinct features in an electrochemical system that attract attention. Of particular interest are potential-induced changes in the structure or the chemical state of SAMs which show a certain degree of reversibility. For example, there is an order–disorder transition in ethanethiol SAMs on Au(111) in 0.1 M H_2SO_4 which is surprisingly reversible:[103] An ordered ethanethiol layer is observed for $E > 0$ V versus SCE (Figure 14a) with domains

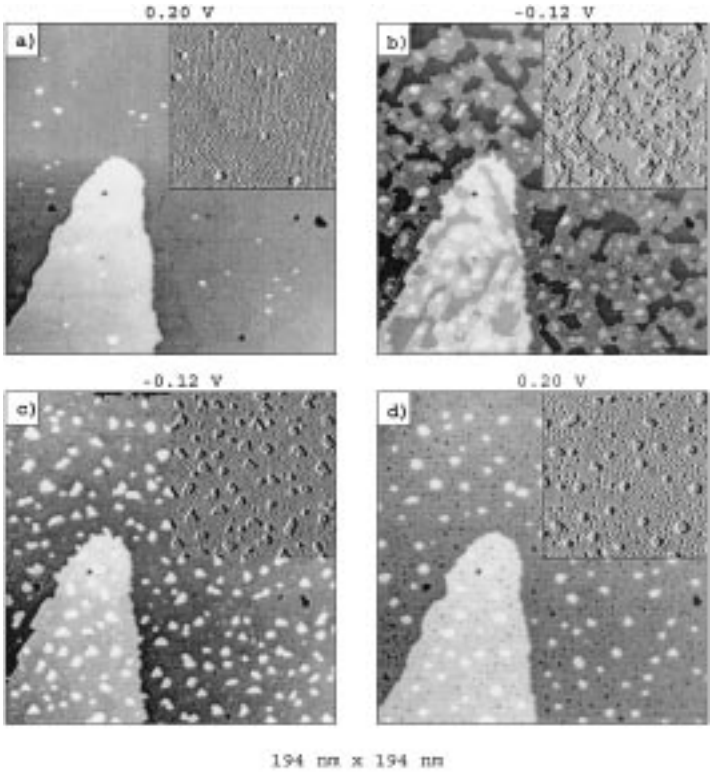

Figure 14. STM images of Au(111) in 0.1 M H_2SO_4 covered with an ethanethiol self-assembled monolayer. The sequence shows the reversible transition between an ordered structure at $+0.20$ V and a disordered one at -0.12 V versus SCE. The upper right corner of the images has been shaded to improve contrast. From ref. [103].

of two distinctly different superstructures (a pinstripe ($p \times \sqrt{3}$) and a densely packed (4×3) structure; see the shadowed top-right quarter of Figure 14a), whereas for $E < -0.1$ V versus SCE a disordered state is found (Figure 14c). The disordered state, which cannot be molecularly resolved in STM images, appears to be less densely packed than the ordered one because small monomolecular high (0.3 ± 0.05 nm) islands are formed in that state, presumably from surface excess. Stepping the potential back to $+0.20$ V versus SCE (Figure 14d) causes the ordered structures (($p \times \sqrt{3}$) and

(4×3) structures) to reappear, albeit in smaller domains and less perfectly ordered. The number of islands has decreased and small holes appear in the surface, to indicate that the extra amount of ethanethiol required for the more densely packed ordered state is only partly supplied by the islands. Hence, the degree of imperfection increases with each structural transition, similar to the case of reconstruction and lifting of reconstruction of gold surfaces.

An interesting complication during the order→disorder transition has been noted and is shown in Figure 14b. The transition produces a striped structure as an intermediate state which exists for a few minutes only and vanishes as the disordered state is completely formed. The stripes are separated by 1.7 nm and are aligned along the three main crystallographic directions of the gold substrate. Upon the potential step from $+0.20$ to -0.12 V versus SCE, first the $(p \times \sqrt{3})$ domains transform into the stripe structure and then the (4×3) structure, which is obviously more stable.

Quite surprisingly, the blocking power of the ethanethiol in the disordered state (for example, against metal deposition) is still high, to indicate that the SAM in the disordered state is also dense. The reversibility of the structure transition for this SAM signals an unexpectedly high surface mobility of these strongly bound molecules. I mention here in passing that the STM is generally assumed to image the sulfur atoms of the thiols rather than the alkane chains or end-substituted functionalized groups.

Another interesting feature of SAM-modified electrodes relates to potential-induced chemical changes of the adlayer. While the oxidative and reductive desorption or destruction of SAMs—deliberately or otherwise—has been frequently studied, investigations of potential-induced changes in the chemical state of SAMs, while they remain intact, are still rare. One such example refers to *p*-nitrothiophenol, which can be partially reduced to *p*-hydroxiaminothiolphenol (Ar-NHOH) by applying a more negative potential. The latter shows a redox behavior due to a reversible switch between Ar-NHOH and Ar-NO, while the former one does not.[104] Successful attempts of a tip-induced (and hence laterally confined) reduction of *p*-nitrothiophenol in a scanning electrochemical microscope cell was reported by Reda,[105] who pursued the idea of a high-density storage device based on switching the oxidation state of single molecules.

A third class of ordered adlayers, which has been intensively studied by STM, comprises metal adsorbates formed by underpotential deposition (upd). The latter expression refers to the formation of a metal monolayer (in rare cases, of two monolayers) on a foreign metal substrate at potentials positive of the corresponding Nernst potential.[106, 107] Such an apparent violation of the Nernst equation simply results from an interaction between adatom and substrate that exceeds in strength that between the adatoms. In a purely thermodynamic rationalization of upd, the activity of the metal $a_{metal} < 1$ has to be assumed.

Copper upd on Au(111) was one of the first systems for which ordered adsorption was shown to occur by structure-sensitive methods, such as ex situ electron diffraction[108] and in situ STM.[109] In sulfuric acid solutions, copper monolayer formation on Au(111) proceeds in three steps: Random adsorption at low coverages, formation of a $(\sqrt{3} \times \sqrt{3})R30^\circ$ superstructure (honeycomb structure with maximum coverage $\Theta_{max} = 2/3$), and finally a pseudomorphic (1×1) copper monolayer, that is, the copper adatoms occupy substrate lattice sites. Because the lattice constant of gold is about 12% larger than that of copper, the pseudomorphic copper layer is strained. An interesting aspect of Cu/Au(111) is that anions play a structure-determining role.[107, 110] The honeycomb structure at medium copper coverages, which is a rather unusual structure for a metal adsorbate, is observed only for sulfate-containing solutions, in which coadsorbed sulfate ions stabilize this structure by nesting in the copper hexagons.[111, 112] Completely different adlayer structures were reported for copper upd in perchloric or chloride solutions.[110]

Figure 15 shows the high-resolution STM image of a submonolayer amount of underpotentially deposited silver on Au(111). Silver upd on Au(111) starts with the successive

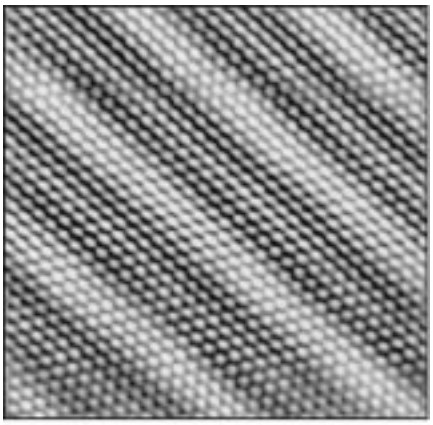

Figure 15. High-resolution STM image of the silver adlayer ($\Theta_{Ag} = 0.37$) on Au(111) in 0.05 M $H_2SO_4 + 1$ mM Ag_2SO_4 at $+0.4$ V versus Ag/Ag^+. From ref. [113].

formation of three different hexagonal adlayer structures: A $(\sqrt{3} \times \sqrt{3})R30^\circ$ arrangement with a limiting coverage of 0.33 ML; a distorted hexagonal-stripe pattern, shown in Figure 15 and which allows coverages up to 0.37 ML; and finally a (3×3) structure with a maximum coverage of 0.44 ML.[113] The distorted hexagonal structure, given in Figure 15, can be obtained from the $(\sqrt{3} \times \sqrt{3})R30^\circ$ lattice by a unidirectional compression of the latter by 10%. The resulting misfit with the underlying substrate surface leads to the height modulation in the adlayer, reflected by the stripes in the STM image. The complete densely packed silver monolayer is (1×1) and free of strain, as silver and gold have practically identical lattice constants. This may also be the reason why a second silver layer even forms in the upd region, although only when very close to the Nernst potential.[113]

6. The Initial Stages of Metal Deposition

Metal plating from solution is still a process of utmost industrial importance. Besides its use in classical areas, such as

protective overcoatings or improvement of the optical appearance of surfaces, electrolytic metal deposition has gained significant attention in various branches of the electronic industry, for example in circuit-board manufacturing, giant-magnetoresistance devices, or metal–semiconductor junctions. While the beginning of metal deposition on a foreign substrate has always been of considerable interest for fundamental research, for example in the study of electrocrystallization phenomena,[114] the initial stages become increasingly relevant also for industrial science as the trend from micro- to nanoelectronics continues with demand for ever smaller products.

Metal deposition is well known to commence at surface defects, which act as nucleation centers for the new phase. Hence, for a detailed study of the nucleation and growth behavior, real-space imaging of the electrode surface is required. In this respect, STM is ideally suited for an atomistic view on the initial stages of metal deposition. Figure 16 shows two STM images of an Au(111) electrode in sulfuric acid

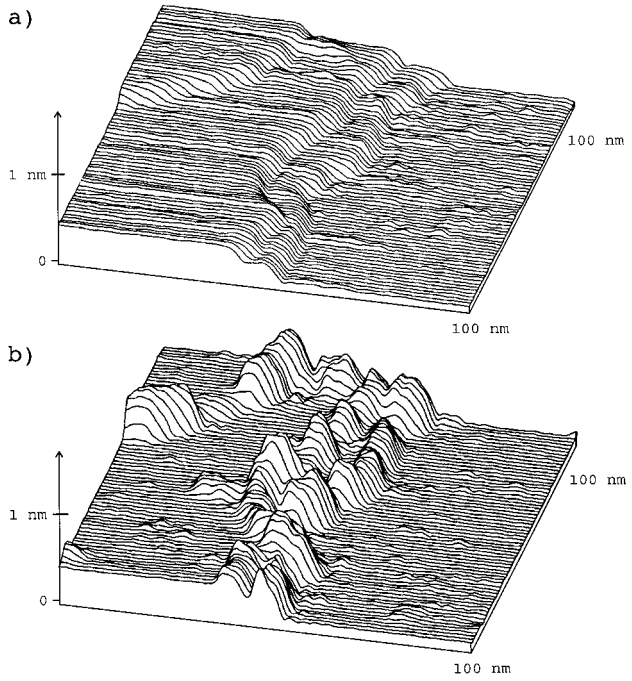

Figure 16. STM images of Au(111) in 5 mM $H_2SO_4 + 0.05$ mM $CuSO_4$ before (a) and during (b) Cu deposition. Nucleation and growth of copper occurs almost exclusively at the steps.

solution before and during deposition of bulk copper. As is clearly seen in Figure 16b, copper nucleates under these conditions almost exclusively at the monoatomic high steps of the gold substrate where the growing copper clusters decorate the surface defects. Substantial amounts of copper can be deposited at the steps while the flat terraces remain essentially copper free (except for the copper monolayer that has been formed at underpotentials and covers the substrate surface uniformly). Such a nucleation-and-growth habit of bulk metal inevitably leads to nonuniform, rough overlayers and hence run counter to the normal intentions of plating industry. There are, however, ways out of this dilemma: Addition of certain groups of organic molecules, "levellers" and "brighteners", can change either the nucleation or the growth behavior of the metal in such a way that smooth overlayers emerge.[115] Although there exist some ideas about the action of additives, the detailed mechanism is still largely unknown; the undeniable successes of the plating industry are a result of trial-and-error and chemical intuition. Nevertheless, this is an important area where STM can and will add significantly to the understanding of additives in the future.[116, 117]

As mentioned above, bulk copper deposition does not start on the bare Au(111) surface but rather on a pseudomorphic copper layer which was formed at underpotentials, namely, positive of the Nernst potential. Due to a considerable lattice mismatch between copper and gold of about 12%, the first monolayer is strained and consequently the next copper atoms are not laid layer-by-layer but instead as clusters, presumably with the native lattice constants. This Stranski–Krastanov growth mode is quite common for metal systems with a lattice misfit: 3D growth on top of a pseudomorphic upd layer. Layer-by-layer growth can be expected, and is indeed experimentally observed, for silver deposition on Au(111) because of the almost perfect match of the lattice parameters for both metals. The result are silver overlayers with large, atomically flat terraces, which even bury rough features of the gold substrate (such as step-bunching regions).[113]

An interesting, yet at first sight puzzling, behavior was reported for copper deposition on Au(100), where again the first monolayer is formed at underpotentials.[118] In this case, a total of ten copper layers was found to grow pseudomorphically, that is, with the lattice constant of gold. A similar observation had been reported earlier for copper on Ag(100), in which exactly eight pseudomorphic layers were grown before a sudden structural transition occurred.[119] The unusually high number of pseudomorphic copper layers on Au(100) and Ag(100), despite the significant lattice misfit, was explained by the growth of body-centered cubic (bcc) rather than face-centered cubic (fcc) copper. Although fcc copper is the thermodynamically most stable form, model calculations have shown that the energy difference between bcc and fcc copper amounts to only 20–40 mV.[120, 121] However, bcc Cu(100) fits almost perfectly onto Au(100) and obviously it is this perfect structural match that favors the initial growth of bcc copper on Au(100). The conclusions from STM measurements were supported by the results of a systematic, in situ surface X-ray scattering (SXS) study.[122] Figure 17 shows the specular reflectivity of bare and copper-covered Au(100) as a function of the scattered wave vector component normal to the surface. The quasi-Bragg peak at $L = 2.8$ results from the bcc copper overlayer. A detailed analysis of the specular reflectivity curves yielded values for the layer spacing in the copper film and for the gold/copper interface: The average copper–copper layer spacing was found to be 0.144 ± 0.002 nm, in good agreement with the expected value for bcc copper and with the STM-derived step heights on the copper overlayer of 0.15 ± 0.01 nm. For the average gold–copper spacing, a value of 0.174 ± 0.010 nm was obtained, which is practically identical to the average of the layer spacings for fcc gold and bcc copper.[122]

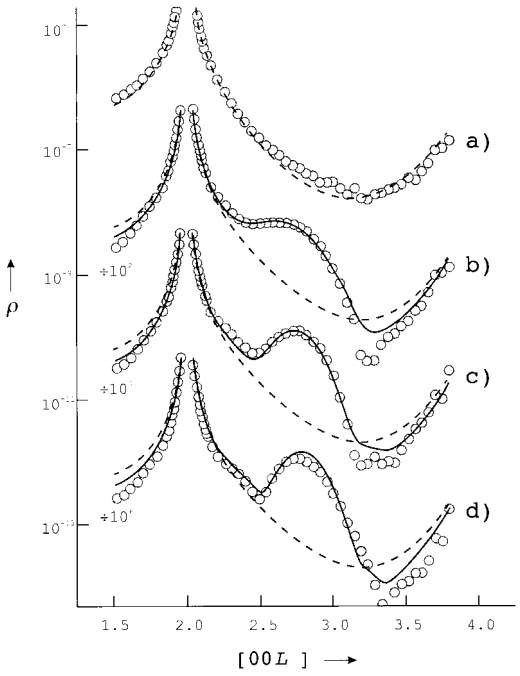

Figure 17. Specular reflectivity ρ of bare (a) and 4.2 (b), 6.7 (c), and 7.9 monolayers (d) of copper covering Au(100) in 0.05 M $H_2SO_4 + 1$ mM $CuSO_4$ as a function of the scattered wave vector component $[00L]$ normal to the surface. The quasi-Bragg peak at $L = 2.8$ is due to bcc Cu. From ref. [122].

With deposition of the eleventh copper layer on Au(100) (of the ninth copper layer on Ag(100)[119]), the surface morphology changes abruptly: The surface appears striped, with a corrugation length of 6.2 ± 0.2 nm for the eleventh layer, 6.5 ± 0.2 nm for the twelfth layer, and a slight increase with each new copper layer. Figure 18 shows an STM image of

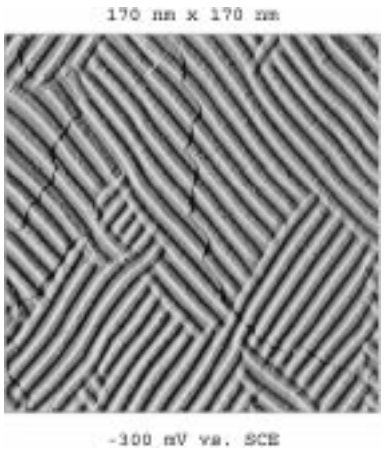

Figure 18. STM image (shaded) of Au(100) in 0.05 M $H_2SO_4 + 1$ mM $CuSO_4$ covered with approximately 13 to 15 Cu monolayers. The Cu overlayer shows the characteristic stripe structure. From ref. [118].

Au(100) covered with 13–15 monolayers of copper. The structure of the wavy overlayer is more difficult to determine. High-resolution STM images indicate a reduction of the copper next-neighbor distance from 0.29 nm in the pseudomorphic layers to 0.26 nm in the ridges of the wavy overlayer.[118, 119] In situ SXS measurements suggest that the wavy overlayer is composed of alternating orthorhombic and cubic stripes.[123]

STM measurements had revealed that after dissolution of the eleventh and higher copper layers on Au(100), the same flat pseudomorphic surface reappeared, which was seen before deposition of the eleventh copper layer. This raised the interesting question about the fate of the ten pseudomorphic copper layers as deposition continues and the wavy structure appears: Do the first ten copper layers remain bcc as the wavy structure grows on top or is the bcc copper transformed into the wavy structure as the eleventh layer is deposited. This question was answered by in situ SXS and the result was quite surprising: With deposition of the eleventh copper layer on Au(100), the entire copper film (namely, all eleven layers) converts into the wavy structure; removal of the eleventh copper layer (or all layers in excess of ten) returns ten pseudomorphic copper layers.[123] The high reversibility of this phenomenon, which shows that the bcc copper overlayer is stable, not just metastable, together with the fact that the structural transition is triggered exactly with the addition or removal of the eleventh layer, makes copper on Au(100) a good example of interesting electrochemical surface science. Not surprisingly, the very same phenomena were observed for copper on Ag(100), at least so far as STM studies are concerned (SXS measurements are still to be performed). Silver and gold have almost identical lattice constants, hence the very same arguments described above also hold for bcc Cu(100) on fcc Ag(100). Actually, the growth of bcc copper was first discovered in UHV studies during copper evaporation onto Ag(100) as substrate.[124] As in the case of Au(100), copper deposition onto Ag(100) starts with the formation of bcc copper until a sudden transition into the wavy structure occurs. Quite remarkably, this transition takes place with laying the ninth copper layer and the pseudomorphic copper reappears as the ninth layer is oxidatively removed. The question remains as to which physical parameters of the substrate are responsible for the difference in critical thickness of the bcc overlayer.

A second example of metal deposition is given in Figure 19.[125] It refers to the initial stages of palladium deposition on Au(111) and emphasizes once more the important role of surface defects, such as monoatomic high steps, as nucleation centers. The sequence of STM images starts with the bare Au(111) surface at $+0.5$ V versus SCE (Figure 19a), which shows one monoatomic high step and several monoatomic high gold islands, leftovers from lifting of the $(22 \times \sqrt{3})$ reconstruction. Stepping the potential to $+0.48$ V versus SCE, that is, into the upd region of palladium, nucleation and growth at the substrate step and at the rims of the gold islands is clearly seen (Figure 19b). Interestingly, there is a slight "chemical" contrast in the STM image, which makes the palladium layer appear higher than the gold, whereas on the basis of geometrical considerations the reverse should be observed. For example, the gold islands, the flat tops of which are still palladium-free, appear darker than the surrounding palladium that has nucleated at the island rims. This contrast is most likely caused by anion adsorption, which will differ for the two metals. As palladium deposition continues in a strictly two-dimensional fashion, the gold terraces become complete-

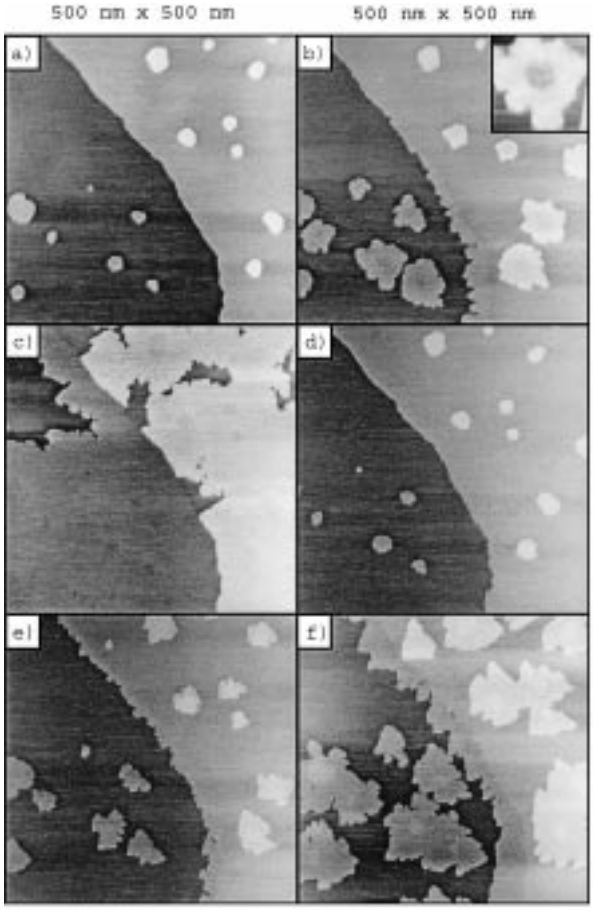

Figure 19. Sequence of STM images ($500 \times 500\ nm^2$) showing the initial stages of Pd deposition onto Au(111) from 0.1 M $H_2SO_4 + 0.1$ mM H_2PdCl_4. Deposition potentials versus SCE: a) +0.55 V (bare gold surface; no Pd deposition); b, c) +0.48 V; d) +0.46 V; e, f) +0.41 V. The inset in (b) has an increased height resolution to show more clearly the chemical contrast between Au (center) and Pd. From ref. [125].

ly covered by palladium nucleating at steps and growing onto the lower terrace, except for the gold islands, which obviously lack nucleation centers. A more negative potential is required to force palladium onto the gold island and the image in Figure 19d is practically identical to that of the bare gold surface (Figure 19a). Now the same process starts again for the second palladium layer, namely nucleation at the monoatomic high step and the island rims (Figures 19e and f). However, before the second layer is complete, the third one begins to grow and, soon after, the fourth layer is formed. Hence, the palladium surface becomes increasingly defect-rich, although the terrace sites are still outnumbering the step sites. This is also reflected in cyclic voltammograms for adsorption processes such as copper upd on the palladium overlayer, which correspond to those for Pd(111) single-crystal electrodes. Thin palladium overlayers on the three low-index faces of gold (and of platinum, to be complete) have been shown to assume the crystallographic orientation of the substrate (if not pseudomorphic), which provides a relatively simple means of obtaining palladium single-crystal surfaces without the troublesome preparation of massive palladium crystals.[126] Thin palladium overlayers have the advantage of showing very little hydrogen absorption,[127] a process which tends to mask other interesting reactions, such as hydrogen adsorption, for massive crystals.

In summarizing the described results, it is obvious that STM is a powerful technique for metal deposition studies, particularly for investigating the very initial stages of this process. The ability of this technique to combine real space imaging with nanometer, if not atomic, resolution leads to structure information of hitherto unprecedented quality which will not only substantially increase our understanding of nucleation and growth on an atomic level but will also be of great value in the attempt to tailor complex surface structures required for future nanotechnologies.

7. Nanostructuring of Electrode Surfaces

The continuing trend in microelectronics for miniaturization has launched a second career of the STM: It is not only a great technique for imaging surfaces with atomic-scale resolution, it is also a tool for positioning single atoms and molecules on surfaces at will and with atomic precision. The tip–substrate interaction at close distances (of the order of an atomic diameter or less), which for surface imaging is a much-feared problem as it may give rise to artifacts, had been successfully employed to move atoms or molecules with the tip along the surface. Impressive examples of this kind of surface nanostructuring have been published by several groups[128–131] which operate under UHV conditions and often at low temperatures; a famous example is Eigler's quantum corral,[132] which consisted of 48 iron atoms on Cu(111) arranged in a circle with the tip of an STM and demonstrated the wave nature of electrons in a very straightforward way.

Work on nanostructuring electrode surfaces started soon after the corresponding experiments in UHV, although the tip-generated entities had to be significantly larger than single atoms in order to survive in an electrochemical environment at room temperature. The first attempts of electrochemical nanostructuring involved tip-induced surface defects, generated either by mechanical contact (tip crashes) or by some sort of sputtering process (initiated by high-voltage pulses between the tip and substrate), which then acted as nucleation centers for metal deposition at predetermined positions.[133, 134] More recently, metal clusters were shown to be positioned on metal and semiconductor surfaces by a two-step process that involved metal deposition from solution onto the STM tip, followed by a burstlike dissolution and redeposition on the sample within a narrow region directly underneath the tip.[135, 136]

In the following, I will describe two different ways of nanostructuring electrode surfaces, as developed in our group, which deal with the spatially confined tip-induced substrate dissolution and tip-induced metal deposition. Two types of tip–substrate interaction, which can lead to the nanostructuring of surfaces, are sketched in Figure 20. Under normal imaging conditions, with typical values of $I_T = 2$ nA and $U_T = 50$ mV, the tip–substrate distance s can be calculated from Equation (3).

$$I_T = R_0^{-1} U_T \exp(-A\sqrt{\phi_T}\, s) \quad (3)$$

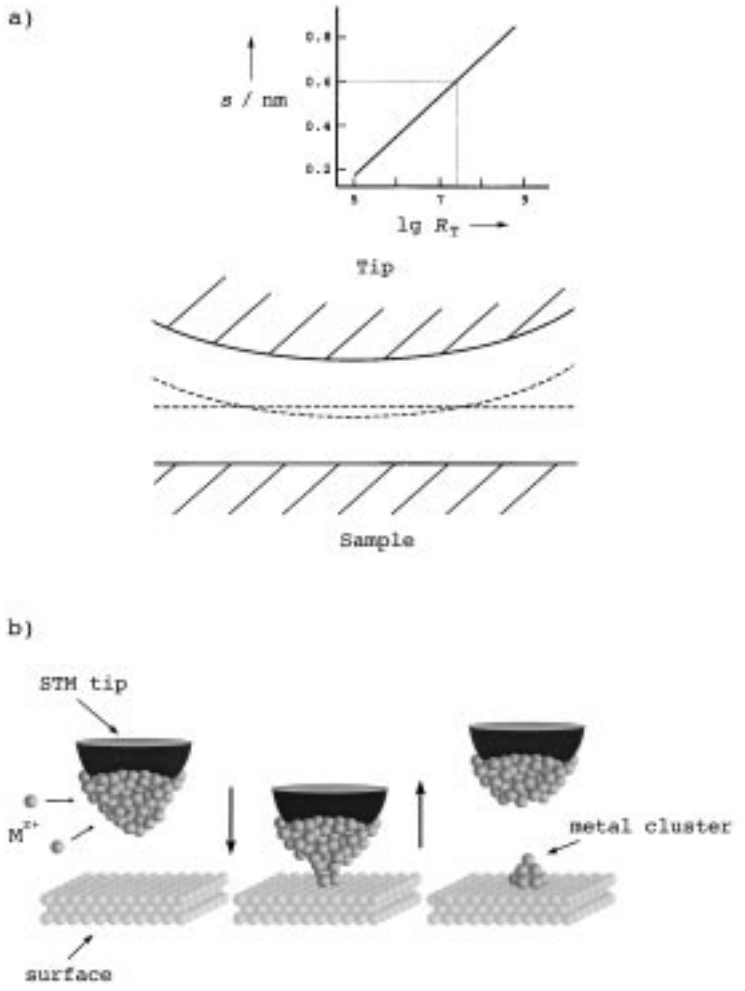

Figure 20. a) Schematic diagram of sample and tip with their electric double layers overlapping. The inset shows the dependence of the tunnel gap s on the tunnel resistance R_T for a tunnel barrier of 1.5 eV. From ref. [138]; b) Schematic representation of the jump-to-contact between a Cu-covered STM tip and an Au substrate. From ref. [139].

The term ϕ_T is the tunnel barrier, $A = 2\sqrt{2m_e}/\hbar = 10.25\ eV^{-1/2}\,nm^{-1}$, and the point-contact resistance $R_0 = 12.90\ k\Omega$. With $\phi_T = 1.5$ eV (typical values of the tunnel barrier at metal/solution interfaces range between 1.0 and 2.0 eV[137]), s equals about 0.6 nm. Considering the fact that the electric double layer of metal electrodes in concentrated solutions is an estimated 0.3 nm thick,[1, 2] the double layers of substrate and tip begin to merge (Figure 20a) and the ideal picture of a noninteracting tip is no longer valid under these conditions. For example, contact with the reference electrode for the imaged area directly underneath the tip may be lost because the bulk electrolyte, which carries the reference potential, has been "squeezed" out. In a recent publication,[138] it was demonstrated that a spatially confined copper dissolution directly underneath the tip can be achieved by applying a tip potential positive of the Cu/Cu^{2+} Nernst potential, despite the fact that the sample potential was held at a value negative of the Cu/Cu^{2+} equilibrium potential. Hence, copper is oxidatively dissolved underneath the tip and only there, although this process should not be possible at that sample potential. This effect is demonstrated in Figure 21 by "drilling" a hole into the Cu(111) surface. After imaging the Cu(111) surface with a tip potential of 0 V versus Cu/Cu^{++} (Figure 21a), the tip was positioned at a fixed location and a potential of +20 mV versus Cu/Cu^{++} applied for 3 min. Although the sample potential was at −50 mV versus Cu/Cu^{++}, a crater 14 nm deep and about 100 nm wide was generated at $I_T = 2$ nA (Figure 21b). Because the tip-induced copper dissolution depended so sensitively on the tip potential relative to the Nernst potential, it was inferred that the copper dissolution under these circumstances was a result of the direct tunneling from the redox system into the empty states of the tip.[138] In this study, it was also shown that there is a smooth transition between imaging without much tip interference and tip-induced surface processing. Depending on the tip and sample potentials, the regimes of 1) tip-enhanced copper deposition, 2) mere surface imaging, or 3) tip-induced copper dissolution will dominate.

Most of the previously published work on nanostructuring deals with the deposition of small metal clusters at predetermined positions. The principle behind our method, which allows the formation of metal clusters in quick succession and without destroying the single crystallinity of the substrate, is as follows.[139, 140] First, metal has to be deposited from solution onto the tip, which is achieved simply by choosing a tip potential negative of the Cu/Cu^{++} equilibrium potential. Second, the metal-loaded tip has to approach the surface for a short period of time, during which a "jump-to-contact" takes place (Figure 20b). This jump-to-contact occurs at close distance between tip and sample (typically 0.3 nm or less) and requires a strong interaction between metal at the tip and substrate to initiate the jump. The resulting connective neck breaks upon the subsequent retraction of the tip, to leave a small metal cluster on the surface. As has been shown before on several occasions, this tip-induced cluster generation has been fully automated, with a microprocessor controlling not only the externally enforced tip approach which leads to the cluster formation but also the x- and y-position of the tip, which allows "writing" complex patterns on the surface.[139] Figure 22 shows an array of 2500 copper clusters on an Au(111) electrode, all about 0.6 nm high, which was accomplished within a few minutes. The clusters were generated by 2 ms voltage pulses to the z-piezo at a repetition rate of 120 Hz. The clusters are remarkably uniform in size and the pattern surmounts monoatomic high steps without any difficulty, to suggest that our technique of nanostructuring works also for slightly rough surfaces. Also noteworthy is the fact that despite the fabrication of many copper clusters at a fairly high rate (the largest array so far consisted of 10000 copper clusters[141]), there is no sign of depletion of copper on the tip. The refilling of the tip during cluster fabrication by the on-going deposition reaction at the tip is surprisingly fast and—quite importantly—retains the high imaging quality of the tip. Therefore,

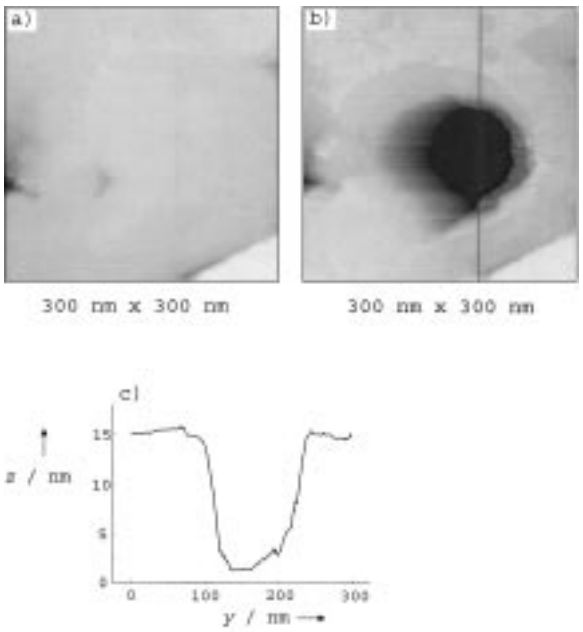

Figure 21. a) STM image of a Cu(111) surface in a Cu^{2+} containing solution at -50 mV versus Cu/Cu^{2+}. $E_{tip} = 0$ V versus Cu/Cu^{2+}. $I_T = 2$ nA. b) Same area, imaged after the tip was held at a fixed position for 3 min at $E_{tip} = +20$ mV versus Cu/Cu^{2+} and $E_{sample} = -50$ mV versus Cu/Cu^{2+}. c) Cross-section along the vertical line shown in (b). From ref. [138].

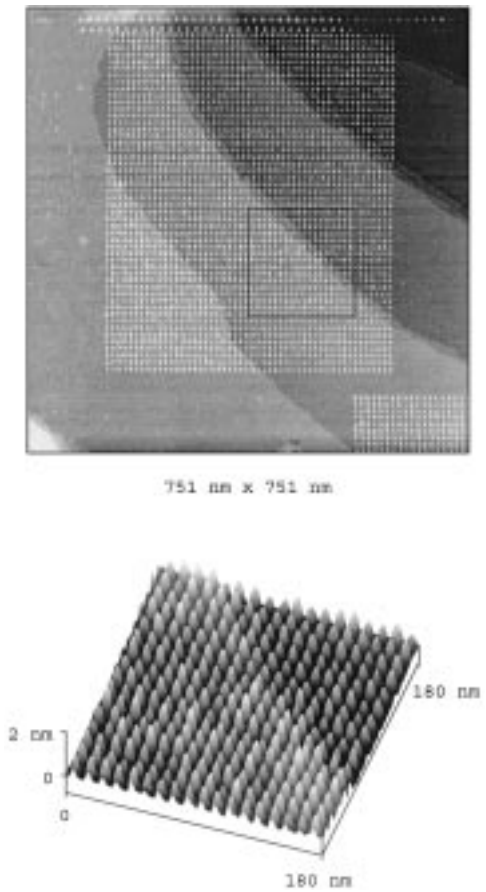

Figure 22. Array of 2500 Cu clusters on Au(111) in 0.05 M $H_2SO_4 + 1$ mM $CuSO_4$, generated by 2500 voltage pulses to the z-piezo. The clusters are about 0.7 nm high. $E_{sample} = +10$ mV versus Cu/Cu^{2+}. The 180×180 nm^2 section of the array demonstrates the uniformity in cluster size. In the top image, two more arrays of tip-induced Cu clusters are visible.

"writing" and "reading" are possible with one and the same tip.

A puzzling feature of the small, tip-induced metal clusters, which contain roughly 100 atoms, is their surprisingly high stability against anodic dissolution. Systematic studies of copper clusters on Au(111) have shown that they are stable at $+10$ mV versus Cu/Cu^{++} for at least one hour and considerably higher "overpotentials", say, 100 mV and more, have to be applied to dissolve the clusters completely.[142] This effect is demonstrated in Figure 23 a, where the height of tip-induced

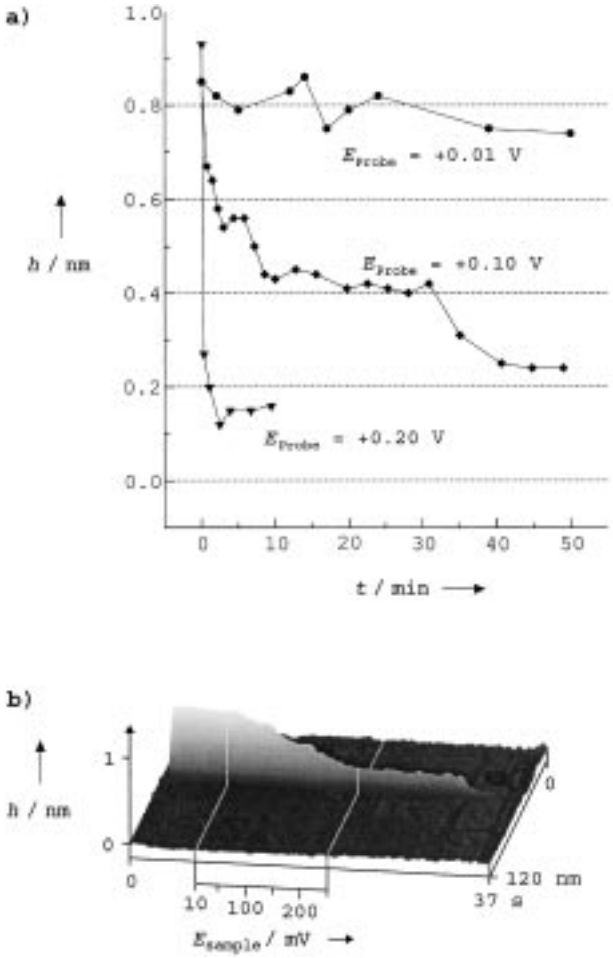

Figure 23. a) Heights h of three tip-induced Cu clusters on Au(111) in 0.05 M $H_2SO_4 + 0.1$ mM $CuSO_4$ as a function of time for three different sample potentials (versus Cu/Cu^{2+}). From ref. [143]. b) Height h of a tip-induced Cu cluster on Au(111) as a function of sample potential. From ref. [143].

clusters is shown as a function of time for different dissolution potentials. At $+100$ mV versus Cu/Cu^{++}, the layer-by-layer dissolution of the cluster is in particular clearly seen. Figure 23 b shows the cluster height as a function of electrode potential, which is scanned from $+10$ mV versus Cu/Cu^{++} (to generate the cluster) to $+250$ mV versus Cu/Cu^{++} (at which the cluster has disappeared completely).[143] Interestingly, there seem to be distinct potential values at which partial dissolution of the clusters occurs. This points towards a quantum-size effect, with a 1 nm high copper cluster being stable up to 50 – 60 mV versus Cu/Cu^{++} and a 0.6 nm high one

even up to about +180 mV versus Cu/Cu^{++}. In comparison, a 2.5 nm high, electrochemically deposited cluster dissolved at +10 mV versus Cu/Cu^{++} within a few seconds and indicates that clusters of that size have bulk properties. However, more experimental data are required to safely establish quantum-size effects in small metal clusters.

8. Conclusions and Outlook

Electrochemical surface science, as a part of physical electrochemistry, has emerged in the endeavor both for an atomistic description of electrode/electrolyte interfaces and for a mechanistic interpretation of electrochemical processes. Significant progress was achieved during the last two decades, mainly through the adoption of experimental approaches and theoretical models of surface physicists. The use of single-crystal electrodes, of nontraditional methods such as in situ X-ray spectroscopies or STM, and of molecular dynamics calculations serve as such examples. Since structural information was most needed to reach our goal, scanning tunneling microscopy has come to play a major role among the many techniques available now to electrochemists. Quite naturally, studies so far were focused on surface structures rather than on dynamical processes or reactions, which would be the ultimate goal in electrochemistry. However, the information about surface reconstruction, about ordered adlayers, and about the initial stages of metal deposition, which has been obtained by STM and was presented here, is indeed amazing. This progress had not been foreseeable 20 years ago.

There are still many open questions that need to be answered. One of the oldest problems in electrochemistry, the structure of the metal/solution interface, is surprisingly far from being solved despite many attempts. The solution side, although handled quite well by theoretical models in the meanwhile, persistently escapes a thorough experimental characterization. This is particularly true for the properties of double-layer water, which are usually masked by those of the adjacent bulk solution. Much was learned from UHV experiments about the water–metal interaction[144] and about the role of hydrogen bonds in determining the structure of water adlayers. There is interesting experimental evidence for high local-field strengths within the electric double layer, revealed, for example, by surface-state spectroscopy, but the various pieces of information still need to be combined to a complete picture. This process, however, seems painfully slow. Much more information is available about the metal side of the double layer, certainly as far as the structures are concerned. This is largely due to STM which indeed has advanced our knowledge in this respect tremendously. The ultimate goal in electrochemistry, however, is a detailed understanding of reactions, namely, electrically driven changes at electrode surfaces. After having investigated the structure for so many years at an atomic level, we will turn to the study of dynamic and kinetic phenomena. This will be a new and important role for the scanning probe microscopies: To adopt the instruments for recording structural changes at millisecond or even briefer time scales. Other techniques, particularly spectroscopic ones, will play a pivotal role, as they are capable of monitoring changes, such as those due to reaction intermediates, at much shorter time scales.

A characteristic feature of electrochemistry always has been its strong and fruitful relation to applied research. Batteries and fuel cells, electrochemical classics, may serve as examples. The study of structure–reactivity relations by employing single-crystal electrodes of different crystallographic orientations or chemically modified by adlayers will be of utmost importance for a better understanding of electrocatalysis, such as for fuel cells. Solid-state ionics play a crucial role in electrochemical sensing as well as high-temperature power sources. Metal deposition from solution, particularly copper deposition, has recently received renewed interest for the fabrication of interconnects in microelectronics and for obtaining layered structures for GMR (giant-magnetoresistance) devices. Metal-deposition studies, especially of the initial stages, on the other hand, have a long tradition in fundamental electrochemistry, namely for looking at electrocrystallization phenomena or ion-transfer reactions.

With the implementation of modern surface-science techniques in electrochemistry and with the increasing awareness of the scientific community about the importance of solid/liquid interfaces (as opposed to, for example, solid/vacuum interfaces), electrochemical surface science in particular and electrochemistry in general has received wide-spread interest and thus, has become a truly interdisciplinary science with strong links to (UHV-based) surface science, organic synthesis, biochemistry, material science, micro- and nanotechnology, sensor technologies, and many others. This is certainly one of the strengths of electrochemistry, which will ensure continued interest in this area. There may be a price to pay: The danger of losing its own identity when the neighboring areas take over the electrochemical part. It will be a challenge for electrochemists to continue to play the central role in the many-faceted field of electrochemistry, which, I am sure, will have a bright future.

It is a pleasure to acknowledge the fruitful collaboration with all my co-workers and visitors of my department.

Received: April 25, 2000 [A 408]

[1] H. Gerischer in *Solid State Electrochemistry* (Eds.: P. J. Gellings, H. J. M. Bouwmeester), CRC, Boca Raton, **1997**, p. 9.
[2] H. Gerischer, D. M. Kolb, J. K. Sass, *Adv. Phys.* **1978**, *27*, 437.
[3] W. Schmickler, *Interfacial Electrochemistry*, Oxford University Press, Oxford, **1996**.
[4] D. C. Grahame, *Chem. Rev.* **1947**, *41*, 441.
[5] R. Parsons, *Adv. Electrochem. Electrochem. Eng.* **1961**, *1*, 1.
[6] D. M. Mohilner, *Electroanal. Chem., Vol. 1* (Ed.: A. J. Bard), Dekker, New York, **1966**, p. 241.
[7] H. Gerischer, *Z. Elektrochem.* **1955**, *59*, 604.
[8] K. J. Vetter, *Elektrochemische Kinetik*, Springer, Berlin, **1961**.
[9] J. O'M. Bockris, M. A. Devanathan, K. Müller, *Proc. R. Soc. London A* **1963**, *274*, 55.
[10] "Surface Science: The First Thirty Years": *Surf. Sci.* **1994**, *299/300*.
[11] G. A. Somorjai, *Introduction to Surface Chemistry and Catalysis*, Wiley, New York, **1994**.
[12] See also the Snowmass Conference **1979** on "Non-Traditional Approaches to the Study of the Solid–Electrolyte Interface": *Surf. Sci.* **1980**, *101*.
[13] D. M. Kolb, *Ber. Bunsenges. Phys. Chem.* **1994**, *98*, 1421.

[14] J. D. E. McIntyre, D. M. Kolb, *Symp. Faraday Soc.* **1970**, *4*, 99.
[15] See, among others: D. M. Kolb in *Spectroelectrochemistry: Theory and Practice* (Ed.: R. J. Gale), Plenum, New York, **1988**, p. 87.
[16] D. L. Jeanmaire, R. P. VanDuyne, *J. Electroanal. Chem.* **1977**, *84*, 1.
[17] A. Bewick, K. Kunimatsu, *Surf. Sci.* **1980**, *101*, 131.
[18] T. Iwasita, F. C. Nart, *Adv. Electrochem. Sci. Eng.* **1995**, *4*, 123.
[19] L. Blum, H. D. Abruña, J. White, J. G. Gordon, G. L. Borges, M. G. Samant, O. R. Melroy, *J. Chem. Phys.* **1986**, *85*, 6732.
[20] O. R. Melroy, M. F. Toney, G. L. Borges, M. G. Samant, J. B. Kortright, P. N. Ross, L. Blum, *J. Electroanal. Chem.* **1989**, *258*, 403.
[21] M. F. Toney, O. R. Melroy in *Electrochemical Interfaces* (Ed.: H. Abruña), VCH, Weinheim, **1991**, p. 55.
[22] J. X. Wang, R. R. Adzic, O. M. Magnussen, B. M. Ocko, *Surf. Sci.* **1995**, *335*, 120.
[23] R. Schumacher, *Angew. Chem.* **1990**, *102*, 347; *Angew. Chem. Int. Ed. Engl.* **1990**, *29*, 329.
[24] V. L. Shannon, D. A. Koos, G. L. Richmond, *J. Chem. Phys.* **1987**, *87*, 1440.
[25] G. L. Richmond, *Adv. Electrochem. Sci. Eng.* **1992**, *2*, 141.
[26] A. Tadjeddine, A. LeRille in *Interfacial Electrochemistry* (Ed.: A. Wieckowski), Dekker, New York, **1999**, p. 317.
[27] P. M. Saville, M. Gonsalves, A. R. Hillman, R. Cubitt, *J. Phys. Chem. B* **1997**, *101*, 1.
[28] Y. Y. Tong, E. Oldfield, A. Wieckowski, *Anal. Chem. A* **1998**, *70*, 518A.
[29] G. Binnig, H. Rohrer, *Helv. Phys. Acta* **1982**, *55*, 726.
[30] G. Binnig, H. Rohrer, *Rev. Mod. Phys.* **1987**, *59*, 615.
[31] R. Sonnenfeld, P. K. Hansma, *Science* **1986**, *232*, 211.
[32] P. Lustenberger, H. Rohrer, R. Christoph, H. Siegenthaler, *J. Electroanal. Chem.* **1988**, *243*, 225.
[33] J. Wiechers, T. Twomey, D. M. Kolb, R. J. Behm, *J. Electroanal. Chem.* **1988**, *248*, 451.
[34] A. T. Hubbard, *Crit. Rev. Anal. Chem.* **1973**, *3*, 201.
[35] W. E. O'Grady, M. Y. C. Woo, P. L. Hagans, E. Yeager, *J. Vac. Sci. Technol.* **1977**, *14*, 365.
[36] F. T. Wagner, P. N. Ross, *J. Electroanal. Chem.* **1983**, *150*, 141.
[37] Y. Nakai, M. S. Zei, D. M. Kolb, G. Lehmpfuhl, *Ber. Bunsenges. Phys. Chem.* **1984**, *88*, 340.
[38] J. Clavilier, R. Faure, G. Guinet, R. Durand, *J. Electroanal. Chem.* **1980**, *107*, 205; J. Clavilier, *J. Electroanal. Chem.* **1980**, *107*, 211.
[39] J. Clavilier, A. Rodes, K. El Achi, M. A. Zamakhchari, *J. Chim. Phys.* **1991**, *88*, 1291.
[40] A. Hamelin, L. Doubova, D. Wagner, H. Schirmer, *J. Electroanal. Chem.* **1987**, *220*, 155.
[41] Y. Uchida, G. Lehmpfuhl, *Surf. Sci.* **1991**, *243*, 193.
[42] N. Batina, A. S. Dakkouri, D. M. Kolb, *J. Electroanal. Chem.* **1994**, *370*, 87.
[43] L. A. Kibler, A. Cuesta, M. Kleinert, D. M. Kolb, *J. Electroanal. Chem.* **2000**, *484*, 73.
[44] D. M. Kolb, J. Schneider, *Electrochim. Acta* **1986**, *31*, 929.
[45] D. M. Kolb in *Structure of Electrified Interfaces* (Eds.: J. Lipkowski, P. N. Ross), VCH, New York, **1993**, p. 65.
[46] J. L. Stickney, I. Villegas, C. B. Ehlers, *J. Am. Chem. Soc.* **1989**, *111*, 6473.
[47] L. B. Goetting, B. M. Huang, T. E. Lister, J. L. Stickney, *Electrochim. Acta* **1995**, *40*, 143.
[48] M. H. Hölzle, T. Wandlowski, D. M. Kolb, *J. Electroanal. Chem.* **1995**, *394*, 271.
[49] E. Yeager, A. Homa, B. D. Cahan, D. Scherson, *J. Vac. Sci. Technol.* **1982**, *20*, 628.
[50] A. T. Hubbard, J. L. Stickney, S. D. Rosasco, M. P. Soriaga, D. Song, *J. Electroanal. Chem.* **1983**, *150*, 165.
[51] J. S. Hammond, N. Winograd, *J. Electroanal. Chem.* **1977**, *80*, 123.
[52] G. C. Allen, P. M. Tucker, A. Capon, R. Parsons, *J. Electroanal. Chem.* **1974**, *50*, 335.
[53] W. N. Hansen, C. L. Wang, T. W. Humpherys, *J. Electroanal. Chem.* **1978**, *90*, 137; W. N. Hansen, C. L. Wang, T. W. Humpherys, *J. Electroanal. Chem.* **1978**, *93*, 87.
[54] J. K. Sass, K. Kretschmar, *Vacuum* **1981**, *31*, 483.
[55] M. S. Zei, G. Lehmpfuhl, D. M. Kolb, *Surf. Sci.* **1989**, *221*, 23.
[56] T. Solomun, B. C. Schardt, S. D. Rosasco, A. Wieckowski, J. L. Stickney, A. T. Hubbard, *J. Electroanal. Chem.* **1984**, *176*, 309.
[57] J. P. Badiali, M. R. Rosinberg, J. Goodisman, *J. Electroanal. Chem.* **1981**, *130*, 31; J. P. Badiali, M. R. Rosinberg, J. Goodisman, *J. Electroanal. Chem.* **1983**, *143*, 73.
[58] W. Schmickler, D. Henderson, *Progr. Surf. Sci.* **1986**, *22*, 323.
[59] E. Spohr, *Adv. Electrochem. Sci. Eng.* **1999**, *6*, 1.
[60] I. Benjamin, *Chem. Rev.* **1996**, *96*, 1449.
[61] E. Spohr, *J. Electroanal. Chem.* **1998**, *450*, 327.
[62] K. Heinzinger in *Structure of Electrified Interfaces* (Eds.: J. Lipkowski, P. N. Ross), VCH, New York, **1993**, p. 246.
[63] P. H. Schmidt, W. J. Plieth, *J. Electroanal. Chem.* **1986**, *201*, 163.
[64] D. M. Kolb, W. Boeck, K. M. Ho, S. H. Liu, *Phys. Rev. Lett.* **1981**, *47*, 1921.
[65] W. Boeck, D. M. Kolb, *Surf. Sci.* **1982**, *118*, 613.
[66] D. M. Kolb, C. Franke, *Appl. Phys. A* **1989**, *49*, 379.
[67] K. M. Ho, C. L. Fu, S. H. Liu, D. M. Kolb, G. Piazza, *J. Electroanal. Chem.* **1983**, *150*, 235.
[68] D. M. Kolb, *Z. Phys. Chem.* **1987**, *154*, 179.
[69] G. Ertl, J. Küppers, *Low Energy Electrons and Surface Chemistry*, VCH, Weinheim, **1985**.
[70] A. T. D'Agostino, W. N. Hansen, *Surf. Sci.* **1986**, *165*, 268.
[71] A. T. D'Agostino, W. N. Hansen, *J. Electron Spectrosc. Relat. Phenom.* **1988**, *46*, 155.
[72] D. M. Kolb, R. Michaelis, *J. Electroanal. Chem.* **1990**, *284*, 507.
[73] U. W. Hamm, V. Lazarescu, D. M. Kolb, *J. Chem. Soc. Faraday Trans.* **1996**, *92*, 3785.
[74] D. Kramer, PhD Thesis, Universität Ulm (Germany), **2000**.
[75] D. L. Rath, D. M. Kolb, *Surf. Sci.* **1981**, *109*, 641.
[76] R. Kötz, H. Neff, K. Müller, *J. Electroanal. Chem.* **1986**, *215*, 331.
[77] W. N. Hansen, D. M. Kolb, *J. Electroanal. Chem.* **1979**, *100*, 493.
[78] G. V. Hansson, S. A. Flodström, *Phys. Rev. B* **1978**, *18*, 1572.
[79] R. Gomer, G. Tryson, *J. Chem. Phys.* **1977**, *66*, 4413.
[80] J. Schneider, C. Franke, D. M. Kolb, *Surf. Sci.* **1988**, *198*, 277.
[81] S. Trasatti, *Pure Appl. Chem.* **1986**, *58*, 955.
[82] V. Heine, L. D. Marks, *J. Electron Spectrosc. Relat. Phenom.* **1986**, *38*, 229; V. Heine, L. D. Marks, *Surf. Sci.* **1986**, *165*, 65.
[83] K. Müller, *Ber. Bunsenges. Phys. Chem.* **1986**, *90*, 184.
[84] G. A. Somorjai, M. A. Van Hove, *Prog. Surf. Sci.* **1989**, *30*, 201.
[85] M. A. Van Hove, R. J. Koestner, P. C. Stair, J. P. Biberian, L. L. Kesmodel, I. Bartos, G. A. Somorjai, *Surf. Sci.* **1981**, *103*, 189; M. A. Van Hove, R. J. Koestner, P. C. Stair, J. P. Biberian, L. L. Kesmodel, I. Bartos, G. A. Somorjai, *Surf. Sci.* **1981**, *103*, 218.
[86] G. Ertl, *Surf. Sci.* **1985**, *152/153*, 328.
[87] D. M. Kolb, *Prog. Surf. Sci.* **1996**, *51*, 109.
[88] A. S. Dakkouri, D. M. Kolb in *Interfacial Electrochemistry* (Ed.: A. Wieckowski), Marcel Dekker, New York, **1999**, p. 151.
[89] A. S. Dakkouri, *Solid State Ionics* **1997**, *94*, 99.
[90] D. M. Kolb, J. Schneider, *Surf. Sci.* **1985**, *162*, 764.
[91] U. W. Hamm, D. M. Kolb, *J. Electroanal. Chem.* **1992**, *332*, 339.
[92] J. Schneider, D. M. Kolb, *Surf. Sci.* **1988**, *193*, 579.
[93] a) H. Striegler, P. Skoluda, D. M. Kolb, *J. Electroanal. Chem.* **1999**, *471*, 9; b) M. Kleinert, A. Cuesta, L. A. Kibler, D. M. Kolb, *Surf. Sci.* **1999**, *430*, L521.
[94] K. Itaya, *Prog. Surf. Sci.* **1998**, *58*, 121.
[95] D. A. Scherson, D. M. Kolb, *J. Electroanal. Chem.* **1984**, *176*, 353.
[96] O. M. Magnussen, B. M. Ocko, R. R. Adzic, J. X. Wang, *Phys. Rev. B* **1995**, *51*, 5510.
[97] Z. Shi, J. Lipkowski, M. Gamboa, P. Zelenay, A. Wieckowski, *J. Electroanal. Chem.* **1994**, *366*, 317.
[98] M. Kleinert, L. A. Kibler, D. M. Kolb, unpublished results.
[99] M. Kunitake, N. Batina, K. Itaya, *Langmuir* **1995**, *11*, 2337.
[100] L.-J. Wan, Y. Hara, H. Noda, M. Osawa, *J. Phys. Chem. B* **1998**, *102*, 5943.
[101] A. Ulman, *Chem. Rev.* **1996**, 96, 1533.
[102] J.-B. D. Green, C. A. McDermott, M. T. McDermott, M. D. Porter in *Imaging of Surfaces and Interfaces* (Eds.: J. Lipkowski, P. N. Ross), Wiley-VCH, New York, **1999**, p. 249.
[103] H. Hagenström, M. A. Schneeweiß, D. M. Kolb, *Langmuir* **1999**, 15, 2435.
[104] H. Tsutsumi, S. Furumoto, M. Morita, Y. Matsuda, *J. Colloid Interface Sci.* **1995**, *171*, 505.
[105] T. Reda, PhD Thesis, Technische Universität München (Germany), **1999**.

[106] D. M. Kolb, *Adv. Electrochem. Electrochem. Eng.* **1978**, *11*, 125.
[107] D. M. Kolb, *Schering Lect. Publ.*, *Vol. 2*, Schering Research Foundation, Berlin, **1991**, p. 1.
[108] H. O. Beckmann, H. Gerischer, D. M. Kolb, G. Lehmpfuhl, *Symp. Faraday Soc.* **1977**, *12*, 51.
[109] O. M. Magnussen, J. Hotlos, G. Beitel, D. M. Kolb, R. J. Behm, *J. Vac. Sci. Technol. B* **1991**, *9*, 969.
[110] M. S. Zei, G. Qiao, G. Lehmpfuhl, D. M. Kolb, *Ber. Bunsenges. Phys. Chem.* **1987**, *91*, 349.
[111] D. A. Huckaby, L. Blum, *J. Electroanal. Chem.* **1991**, *315*, 255.
[112] M. F. Toney, J. N. Howard, J. Richer, G. L. Borges, J. G. Gordon, O. R. Melroy, D. Yee, L. B. Sorensen, *Phys. Rev. Lett.* **1995**, *75*, 4472.
[113] M. J. Esplandiu, M. A. Schneeweiß, D. M. Kolb, *Phys. Chem. Chem. Phys.* **1999**, *1*, 4847.
[114] E. Budevski, G. Staikov, W. J. Lorenz, *Electrochemical Phase Formation and Growth*, VCH, Weinheim, **1996**.
[115] H. Fischer, *Elektrolytische Abscheidung und Elektrokristallisation von Metallen*, Springer, Berlin, **1954**.
[116] R. J. Nichols, C. E. Bach, H. Meyer, *Ber. Bunsenges. Phys. Chem.* **1993**, *97*, 1012.
[117] M. A. Schneeweiß, H. Hagenström, M. J. Esplandiu, D. M. Kolb, *Appl. Phys. A* **1999**, *69*, 537.
[118] R. Randler, M. Dietterle, D. M. Kolb, *Z. Phys. Chem.* **1999**, *208*, 43.
[119] M. Dietterle, T. Will, D. M. Kolb, *Surf. Sci.* **1998**, *396*, 189.
[120] J. R. Chelikowsky, M. Y. Chou, *Phys. Rev. B* **1988**, *38*, 7966.
[121] T. Kraft, P. M. Marcus, M. Methfessel, M. Scheffler, *Phys. Rev. B* **1993**, *48*, 5886.
[122] R. J. Randler, D. M. Kolb, B. M. Ocko, I. K. Robinson, *Surf. Sci.* **2000**, *447*, 187.
[123] B. M. Ocko, I. K. Robinson, M. Weinert, R. J. Randler, D. M. Kolb, *Phys. Rev. Lett.* **1999**, *83*, 780.
[124] W. F. Egelhoff, I. Jacob, *Phys. Rev. Lett.* **1989**, *62*, 921.
[125] L. A. Kibler, M. Kleinert, R. Randler, D. M. Kolb, *Surf. Sci.* **1999**, *443*, 19.
[126] M. Baldauf, D. M. Kolb, *J. Phys. Chem.* **1996**, *100*, 11375.
[127] M. Baldauf, D. M. Kolb, *Electrochim. Acta* **1993**, *38*, 2145.
[128] D. M. Eigler, E. K. Schweizer, *Nature* **1990**, *344*, 524.
[129] Ph. Avouris, I.-W. Lyo, *Appl. Surf. Sci.* **1992**, *60/61*, 426.
[130] G. Meyer, S. Zöphel, K. H. Rieder, *Appl. Phys. A* **1996**, *63*, 557.
[131] M. T. Cuberes, R. R. Schlittler, J. K. Gimzewski, *Surf. Sci.* **1997**, *371*, L231.
[132] M. F. Crommie, C. P. Lutz, D. M. Eigler, *Science* **1992**, *262*, 218.
[133] W. Li, J. A. Virtanen, R. M. Penner, *J. Phys. Chem.* **1992**, *96*, 6529.
[134] W. Li, G. S. Hsiao, D. Harris, R. M. Nyffenegger, J. A. Virtanen, R. M. Penner, *J. Phys. Chem.* **1996**, *100*, 20103.
[135] W. Schindler, D. Hofmann, J. Kirschner, *J. Appl. Phys.* **2000**, *87*, 7007.
[136] R. T. Pötzschke, G. Staikov, W. J. Lorenz, W. Wiesbeck, *J. Electrochem. Soc.* **1999**, *146*, 141.
[137] G. E. Engelmann, PhD Thesis, Universität Ulm (Germany), **1997**.
[138] Z.-X. Xie, D. M. Kolb, *J. Electroanal. Chem.* **2000**, *481*, 177.
[139] D. M. Kolb, R. Ullmann, T. Will, *Science* **1997**, *275*, 1097.
[140] D. M. Kolb, R. Ullmann, J. C. Ziegler, *Electrochim. Acta* **1998**, *43*, 2751.
[141] G. E. Engelmann, J. C. Ziegler, D. M. Kolb, *Surf. Sci.* **1998**, *401*, L420.
[142] R. Ullmann, T. Will, D. M. Kolb, *Ber. Bunsenges. Phys. Chem.* **1995**, *99*, 1414.
[143] D. M. Kolb, G. E. Engelmann, J. C. Ziegler, *Angew. Chem.* **2000**, *112*, 1166; *Angew. Chem. Int. Ed.* **2000**, *39*, 1123.
[144] P. A. Thiel, T. E. Madey, *Surf. Sci. Rep.* **1987**, *7*, 211.